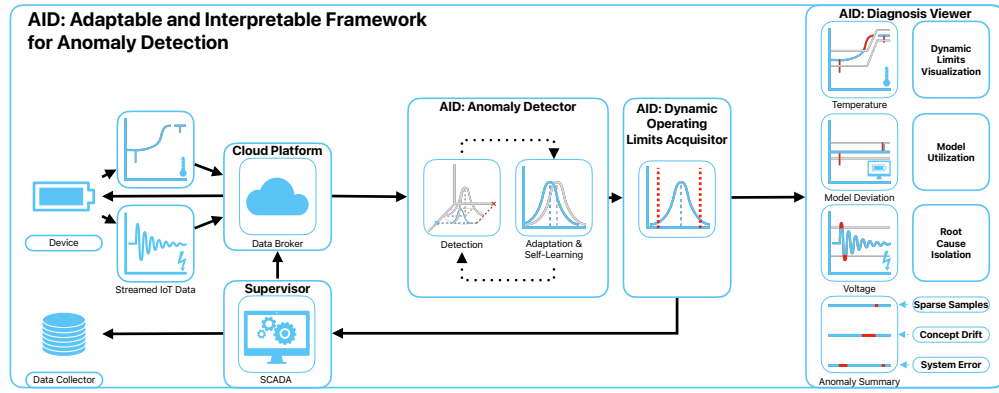


# Graphical Abstract

## Adaptable and Interpretable Framework for Anomaly Detection in SCADA-based Industrial Systems

Marek Wadinger, Michal Kvasnica



## Highlights

### **Adaptable and Interpretable Framework for Anomaly Detection in SCADA-based Industrial Systems**

Marek Wadinger, Michal Kvasnica

- Interpretable anomaly detector with self-supervised adaptation
- Demonstrates interpretability by providing dynamic operating limits
- Leverages self-learning approach on streamed IoT data
- Utilizes existing SCADA-based industrial infrastructure
- Offers faster response time to incidents due to root cause isolation

# Adaptable and Interpretable Framework for Anomaly Detection in SCADA-based Industrial Systems

Marek Wadinger<sup>a,b,\*</sup>, Michal Kvasnica<sup>a,b</sup>

<sup>a</sup>*Institute of Information Engineering, Automation and Mathematics, Slovak University of Technology in Bratislava, Radlinskeho 9, 812 37, Bratislava, Slovakia*

<sup>b</sup>*Tesla Labs s.r.o., Pálenica 53/79, 033 17, Liptovský Hrádok, Slovakia*

---

## Abstract

In this paper, we introduce an Adaptable and Interpretable Framework for Anomaly Detection (AID) designed for industrial systems utilizing IoT data streams on top of well-established SCADA systems. AID leverages dynamic conditional probability distribution modeling to capture the normal operation of dynamic systems and isolate the root causes of anomalies at the level of individual inputs. The self-supervised framework dynamically updates parameters of underlying model, allowing it to adapt to non-stationarity. AID interprets anomalies as significant deviations from conditional probability, encompassing interactions as well as both spatial and temporal irregularities by exposing them as features. Crucially, AID provides dynamic operating limits to integrate with existing alarm handling mechanisms in SCADA-based IoT systems. Two industrial-scale case studies demonstrate AID's capabilities. The first study showcases AID's effectiveness on energy storage system, adapting to changes, setting context-aware limits for SCADA, and ability to leverage a physics-based model. The second study monitors battery module temperatures, where AID identifies hardware faults, emphasizing its relevance to energy storage safety. A benchmark evaluation on real data shows that AID delivers comparable performance to other self-learning adaptable anomaly detection methods, with the significant advancement in diagnostic capabilities for improved system reliability and performance.

*Keywords:* Anomaly detection, Root cause isolation, Iterative learning,

---

\*Phone numbers: +421 902 810 324 (Marek Wadinger)

Email addresses: [marek.wadinger@stuba.sk](mailto:marek.wadinger@stuba.sk) (Marek Wadinger), [michal.kvasnica@stuba.sk](mailto:michal.kvasnica@stuba.sk) (Michal Kvasnica)

## **1. Introduction**

Anomaly detection systems play a critical role in risk-averse systems by identifying abnormal patterns and adapting to novel expected patterns in data. These systems are particularly vital in the context of Internet of Things (IoT) devices that continuously stream high-fidelity data to control units.

In this rapidly evolving field with long-spanning roots, Chandola et al. (2009) conducted an influential review of prior research efforts across diverse application domains. Recent studies have underscored the need for holistic and tunable anomaly detection methods accessible to operators (Laptev et al., 2015; Kejariwal, 2015; Cook et al., 2020).

Cook et al. denote substantial aspects that pose challenges to anomaly detection in IoT, including the temporal, spatial, and external context of measurements, multivariate characteristics, noise, and nonstationarity (Cook et al., 2020). To address these complexity issues, Zhang et al. (2024) have successfully employed spatially distributed sensors and time-relative modulation. Their approach has proven effective, particularly in the context of complex non-linear systems, offering potential solutions to some of the challenges posed by IoT data. Huang et al., on the other hand, tackled the problems of detecting global outliers, local outliers, and outlier clusters simultaneously. Their proposed approach, based on density estimation, relies on the notion that density distributions should exhibit minimal variations in local areas. To achieve this, they introduce a novel turning ratio metric, which reduces reliance on hyperparameters and enhances anomaly detection (Huang et al., 2023).

Additionally, feature engineering techniques play a crucial role in capturing contextual properties and enhancing anomaly detection performance (Fan et al., 2019). However, it is worth noting that feature engineering may introduce categorical variables and significantly increase the dimensionality of the data, requiring specific methods for handling large data, sizeable data storage, and substantial computational resources (Talagala et al., 2021). Recently, Li et al. introduced an attribute-weighted outlier detection algorithm, designed for high-dimensional datasets with mixtures of categorical and numerical data. Their approach assigns different weights to individual attributes based on their importance in anomaly detection and uses

35 these weights to calculate distances between data points. Notably, Li et  
36 al. demonstrated the superior performance of their algorithm compared to  
37 state-of-the-art methods (Li and Liu, 2024). Another strategy for handling  
38 high-dimensional data involves using deep learning methods with synthetic  
39 normal data to enhance the detection of outliers with subtle deviations, as  
40 proposed in Du et al. (2024).

41 Nevertheless, the presence of nonstationarity, often stemming from con-  
42 cept drift (a shift in data patterns due to changes in statistical distribution)  
43 and change points (permanent alterations in system state), presents a sub-  
44 stantial challenge (Salehi and Rashidi, 2018). In practical scenarios, those  
45 changes tend to be unpredictable in both their spatial and temporal aspects.  
46 Consequently, they require systems with solid outlier rejection capabilities of  
47 intelligent tracking algorithms (Barbosa Roa et al., 2019). This underscores  
48 the critical importance of an anomaly detection method’s ability to adapt to  
49 evolving data structures, especially in long-term deployments. Nevertheless,  
50 as (Tartakovsky et al., 2013) remarked, immediate detection is not a feasible  
51 option unless there is a high tolerance for false alarms.

52 The adaptation of batch models at scale introduces a significant latency in  
53 detector adaptation (Wu et al., 2021). Incremental learning methods allowed  
54 adaptation while restraining the storage of the whole dataset. The super-  
55 vised operator-in-the-loop solution offered by Pannu et al. (2012) showed  
56 the detector’s adaptation to data labeled on the flight. Others approached  
57 the problem as sequential processing of bounded data buffers in univariate  
58 signals (Ahmad et al., 2017) and multivariate systems (Bosman et al., 2015).

### 59 1.1. Related Work

60 Recent advances in anomaly detection have broadened its scope to include  
61 root cause identification governed by the development of explanatory meth-  
62 ods capable of diagnosing and tracking faults across the system. Studies can  
63 be split into two groups of distinct approaches. The first group approaches  
64 explainability as the importance of individual features (Carletti et al., 2019;  
65 Nguyen et al., 2019; Amarasinghe et al., 2018). Those studies allow an expla-  
66 nation of novelty by considering features independently. The second group  
67 uses statistical learning creating models explainable via probability. For in-  
68 stance, the integration of variational Bayesian inference probabilistic graph  
69 neural network allowed Zhang et al. to model the posterior distribution  
70 of sensor dependency for gas leakage localization on unlabeled data (Zhang  
71 et al., 2023). Yang et al. recently proposed a Bayesian network (BN) for fault

72 detection and diagnosis. In this BN, individual nodes of the network represent  
73 normally distributed variables, whereas the multiple regression model defines weights and relationships. Using the predefined structure of the BN,  
74 the authors propose offline training with online detection and diagnosis (Yang et al., 2022).

75 Given the infrequent occurrence of anomalies and their potential absence in training data, the incorporation of synthetic data or feature extraction for various detected events emerges to assist diagnosis of the system. Brito et al. designed synthetic faults based on expert knowledge and introduced them into a transfer learning classifier to exploit faults in rotating machinery, with a subsequent explanation layer (Brito et al., 2023). Conversely, We et al. leveraged feature selection to expose various types of abnormal behavior. The team presents competitive performance while using change in relationships to provide causal inference (Wu et al., 2024).

76 However, it is crucial to underscore that offline training, as previously emphasized, is inherently inadequate when it comes to adapting to anticipated novel patterns, rendering it unsuitable for sustained, long-term operation on IoT devices.

77 This paper emphasizes the importance of combining adaptability in interpretable anomaly detection and proposes a method that addresses this challenge in real industrial systems. Here we report the discovery and characterization of an adaptive anomaly detection method for existing supervisory control and data acquisition (SCADA) systems, employing streaming IoT data. The ability to diagnose multivariate data while providing root cause isolation via statistical learning, extends our previous contribution to the field as presented in (Wadinger and Kvasnica, 2023). The proposed algorithm aims to represent a general method that aids a range of existing safety-critical systems where anomaly diagnosis and identification are paramount.  
78 The schematic overview of the proposed method’s integration is presented in Figure 1.

### 79 1.2. Novelty of proposed approach

80 The idea of using statistical outlier detection is well-established. We highlight the impactful contributions of Yamanishi et al. in (Yamanishi and Takeuchi, 2002; Yamanishi et al., 2004). The authors propose a method for detecting anomalies in a time series. The method is based on the assumption that the continuous data is generated by a mixture of Gaussian distributions, while discrete data is modeled as histogram density. The authors solve the

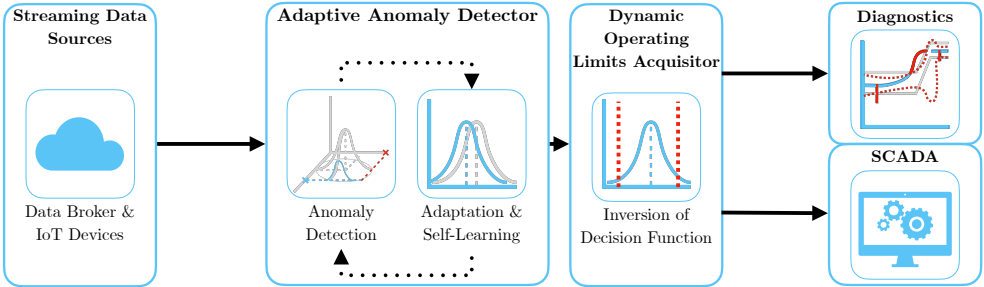


Figure 1: Schematic representation of the proposed method AID.

109 problem of change point detection as well. However, the adaptation sys-  
 110 tem is unaware of such changes, making the moving window the only source  
 111 of adaptation. Our self-supervised approach facilitates intelligent adaptation  
 112 concerning detected change points, to increase the speed of adaptation where  
 113 the probability of concept drift is high. By leveraging its ability to adapt to  
 114 changes in operational states, our proposed method operates autonomously  
 115 when such changes occur. Moreover, Yamanishi et al. (2004) does not at-  
 116 tempt to isolate the root cause of the anomaly. Our approach extends statis-  
 117 tical outlier detection by incorporating interpretability. This is achieved by  
 118 evaluating the inverse cumulative distribution function of the latest condi-  
 119 tional probabilities for each measurement, considering the remainder of the  
 120 measurements, and establishing limits that define the threshold for normal  
 121 event probabilities.

122 A limited number of studies have focused on adaptation and interpretabil-  
 123 ity within the framework of anomaly detection. Two recent contributions in  
 124 this area are made by Steenwinckel et al. as reported in (Steenwinckel, 2018;  
 125 Steenwinckel et al., 2021). In Steenwinckel (2018), the authors emphasize  
 126 the importance of combining prior knowledge with a data-driven approach  
 127 to achieve interpretability, particularly concerning root cause isolation. They  
 128 propose a novel approach that involves extracting features based on knowl-  
 129 edge graph pattern extraction and integrating them into the anomaly de-  
 130 tection mechanism. This graph is subsequently transformed into a matrix,  
 131 and adaptive region-of-interest extraction is performed using reinforce-  
 132 learning techniques. To enhance interpretability, a Generative Adversarial  
 133 Network (GAN) reconstructs a new graphical representation based on se-  
 134 lected vectors. However, it is important to note that the validation of this

idealized approach is pending further investigation. Lately, Steenwinckel et al. (2021) introduced a comprehensive framework for adaptive anomaly detection and root cause analysis in data streams. While the adaptation process is driven by user feedback, the specific mechanism remains undisclosed. The authors present an interpretation of their method through a user dashboard, featuring visualizations of raw data. This dashboard is capable of distinguishing between track-related problems and train-related issues, based on whether multiple trains at the same geographical location approach the anomaly. Meanwhile, our efforts are directed towards the development of a self-supervised method that can learn autonomously, reducing the reliance on human supervision, which is often constrained by time limitations and can lead to significant delays in adaptation. Our method is distinguished by its straightforward statistical reasoning and the ability to isolate the root cause of anomalies. The interpretability of our method is demonstrated through the establishment of dynamic operating limits for each signal, leveraging conditional probabilities derived from the signal and other system measurements and features. This provides operators with a clear understanding of the system's state and the underlying causes of anomalies and offers interoperability with existing alarm handling mechanisms in SCADA which utilize operating limits. To the best of our knowledge, this study appears to be one of the initial attempts to introduce a self-supervised approach for adaptive anomaly detection and root cause isolation in SCADA-based systems utilizing IoT data streams.

### 1.3. Validation

Two real-world industrial-scale case studies showcase that our proposed method has the capacity to explain anomalies, isolate the root cause, and allow adaptation to change points, allowing long-term deployment at the end users of energy storage systems. We observe similar detection performance, albeit with lower scalability, on benchmark data when comparing our approach to well-established unsupervised anomaly detection methods in streamed data which create a bedrock for many state-of-the-art contributions, such as One-Class SVM (Amer et al., 2013; Liu et al., 2014; Krawczyk and Woźniak, 2015; Miao et al., 2019; Gözüaçık and Can, 2021), and Half-Space Trees (Wetzig et al., 2019; Lyu et al., 2020).

169 *1.4. Practical Impact*

170 Potential applications of the proposed method are in the field of energy  
171 storage systems, where the ability to detect anomalies and isolate their root  
172 causes while adapting to changes in operation and environment, is crucial  
173 for the system safety. The proposed method is designed to be integrated  
174 into the existing infrastructure of the systems, utilizing IoT data streams on  
175 top of well-established SCADA systems. SCADA systems continuously mon-  
176 itor these process data in real-time, embodying alarm handling mechanisms,  
177 which are designed to notify operators of the system's abnormal behavior  
178 and drive attention to the root of the problem. By comparing the current  
179 values to the upper and lower operating limits, they take action when a  
180 variable exceeds or falls below these limits. However, safe operating limits  
181 are often established based on a combination of equipment design limits and  
182 the dynamics of the process (Stauffer and Chastain-Knight, 2021). Those  
183 are indifferent to the actual state of the system and environmental condi-  
184 tions. The proposed method allows the establishment of dynamic operating  
185 limits, based on the current state of the system and its environment, with  
186 direct utilization in SCADA systems expecting minimal intervention to exist-  
187 ing infrastructure. This allows the system to operate closer or further from  
188 its design limits, increasing its safety and profitability. The dynamic op-  
189 erating limits allow operational metrics monitoring, making potential early  
190 detection and prevention easier. Using general adaptable methods without  
191 interpretability, on the other hand, may pose safety risks and lower total  
192 financial benefits, as the triggered false alarms may need to be thoroughly  
193 analyzed, resulting in prolonged downtimes.

194 The main contribution of the proposed solution to the developed body of  
195 research is that it:

- 196     • Interpretable anomaly detector with self-supervised adaptation
- 197     • Demonstrates interpretability by providing dynamic operating limits
- 198     • Leverages self-learning approach on streamed IoT data
- 199     • Utilizes existing SCADA-based industrial infrastructure
- 200     • Offers faster response time to incidents due to root cause isolation

201    1.5. Paper Organization

202    The rest of the paper is structured as follows: We begin with the problem  
203    and motivation in **Section 1**, providing context. Next, in **Section 2**, we  
204    lay the theoretical groundwork. Our proposed adaptive anomaly detection  
205    method is detailed in **Section 3**. We then demonstrate real-world industrial-  
206    scale applications in **Section 4**. Finally, we conclude the paper in **Section 5**,  
207    summarizing findings and discussing future research directions.

208    2. Preliminaries

209    In this section, we present the fundamental ideas that form the basis  
210    of the developed approach. Subsection 2.1 explains Welford's online algo-  
211    rithm, which can adjust distribution to changes in real-time. Subsection 2.2  
212    proposes a two-pass implementation that can reverse the impact of expired  
213    samples. The math behind distribution modeling in Subsection 2.3 estab-  
214    lishes the foundation for the Gaussian anomaly detection model discussed in  
215    Subsection 2.5, followed by conditional probability computation in Subsec-  
216    tion 2.4. The last subsection of the preliminaries is devoted to the definition  
217    of anomalies.

218    2.1. Welford's Online Algorithm

219    Welford introduced a numerically stable online algorithm for calculating  
220    mean and variance in a single pass through data. Therefore, the algorithm  
221    allows the processing of IoT device measurements without the need to store  
222    their values (Welford, 1962).

223    Given measurement  $x_i$  where  $i = 1, \dots, n$  is a sample index in sample  
224    population  $n$ , the corrected sum of squares  $S_n$  is defined as

$$S_n = \sum_{i=1}^n (x_i - \bar{x}_n)^2, \quad (1)$$

225    with the running mean  $\bar{x}_n$  defined as previous mean  $\bar{x}_{n-1}$  weighted by pro-  
226    portion of previously seen population  $n - 1$  corrected by current sample as

$$\bar{x}_n = \frac{n-1}{n} \bar{x}_{n-1} + \frac{1}{n} x_n = \bar{x}_{n-1} + \frac{x_n - \bar{x}_{n-1}}{n}. \quad (2)$$

227    Throughout this paper, we consider the following formulation of an update  
228    to the corrected sum of squares:

$$S_n = S_{n-1} + (x_n - \bar{x}_{n-1})(x_n - \bar{x}_n), \quad (3)$$

as it is less prone to numerical instability due to catastrophic cancellation, significant loss of precision due to subtracting two nearly equal numbers. Finally, the corresponding unbiased variance is

$$s_n^2 = \frac{S_n}{n - 1}. \quad (4)$$

This implementation of the Welford method requires the storage of three scalars:  $\bar{x}_{n-1}$ ;  $n$ ;  $S_n$ .

### 2.2. Inverting Welford's Algorithm

Based on (2), it is clear that the influence of the latest sample over the running mean decreases as the population  $n$  grows. For this reason, regulating the number of samples used for sample mean and variance computation has crucial importance over adaptation. Given access to the instances used for computation and expiration period  $t_e \in \mathbb{N}_0^{n-1}$ , reverting the impact of  $x_{n-t_e}$  can be written as follows

$$S_{n-1} = S_n - (x_{n-t_e} - \bar{x}_{n-1})(x_{n-t_e} - \bar{x}_n), \quad (5)$$

where the reverted mean is given as

$$\bar{x}_{n-1} = \frac{n}{n-1}\bar{x}_n - \frac{1}{n-1}x_{n-t_e} = \bar{x}_n - \frac{x_{n-t_e} - \bar{x}_n}{n-1}. \quad (6)$$

Finally, the unbiased variance follows the formula:

$$s_{n-1}^2 = \frac{S_{n-1}}{n-2}. \quad (7)$$

Notably, inversion allows the algorithm to keep a constant rate of adaptation at the cost of storing a bounded data buffer.

### 2.3. Statistical Model of Multivariate System

Multivariate normal distribution generalizes the multivariate systems to the model where the degree to which variables are related is represented by the covariance matrix. Gaussian normal distribution of variables is a reasonable assumption for process measurements, as it is a common distribution that arises from stable physical processes measured with noise (Mishra and Datta-Gupta, 2018). The general notation of multivariate normal distribution is:

$$\mathbf{X} \sim \mathcal{N}_k(\boldsymbol{\mu}, \boldsymbol{\Sigma}), \quad (8)$$

253 where  $k$ -dimensional mean vector is denoted as  $\boldsymbol{\mu} = (\bar{x}_1, \dots, \bar{x}_k)^T \in \mathbb{R}^k$   
 254 and  $\boldsymbol{\Sigma} \in \mathbb{R}^{k \times k}$  is the  $k \times k$  covariance matrix, where  $k$  is the index of last  
 255 random variable.

256 The probability density function (PDF)  $f(\mathbf{x}; \boldsymbol{\mu}, \boldsymbol{\Sigma})$  of multivariate normal  
 257 distribution is denoted as:

$$f(\mathbf{x}; \boldsymbol{\mu}, \boldsymbol{\Sigma}) = \frac{1}{(2\pi)^{k/2} |\boldsymbol{\Sigma}|^{1/2}} e^{-\frac{1}{2}(\mathbf{x}-\boldsymbol{\mu})^\top \boldsymbol{\Sigma}^{-1}(\mathbf{x}-\boldsymbol{\mu})}, \quad (9)$$

258 where  $\mathbf{x}$  is a  $k$ -dimensional vector of measurements  $x_i$  at time  $i$ ,  $|\boldsymbol{\Sigma}|$   
 259 denotes the determinant of  $\boldsymbol{\Sigma}$ , and  $\boldsymbol{\Sigma}^{-1}$  is the inverse of  $\boldsymbol{\Sigma}$ .

260 The cumulative distribution function (CDF) of a multivariate Gaussian  
 261 distribution describes the probability that all components of the random  
 262 vector  $\mathbf{X}$  take on a value less than or equal to a particular point  $q$  in space,  
 263 and can be used to evaluate the likelihood of observing a particular set of  
 264 measurements or data points. In other words, it gives the probability of  
 265 observing a random vector that falls within a certain region of space. The  
 266 standard notation of CDF is as follows:

$$F(\mathbf{x}; \boldsymbol{\mu}, \boldsymbol{\Sigma}) = \int_{-\infty}^q f(\mathbf{x}; \boldsymbol{\mu}, \boldsymbol{\Sigma}) d\mathbf{x}, \quad (10)$$

267 where  $d\mathbf{x}$  denotes the integration over all  $k$  dimensions of  $\mathbf{x}$ .

268 As the equation (10) cannot be integrated explicitly, an algorithm for  
 269 numerical computation was proposed in Genz (2000).

270 Given the PDF, we can also determine the value of  $\mathbf{x}$  that corresponds to a  
 271 given quantile  $q$  using a numerical method for inversion of CDF (ICDF) often  
 272 denoted as percent point function (PPF) or  $F(\mathbf{x}; \boldsymbol{\mu}, \boldsymbol{\Sigma})^{-1}$ . An algorithm that  
 273 calculates the value of the PPF is part of standard statistical software tools.

#### 274 2.4. Conditional Probability Distribution

275 Considering that we observe particular vector  $\mathbf{x}_i$ , we can update probability  
 276 distributions, calculated according to the rules of conditional probability,  
 277 of individual measurements within the vector given the rest of the measurements  
 278 in  $\mathbf{x}_i$ . Let's assume multivariate normal distribution (8) and without  
 279 loss of generality, that the vector  $\mathbf{x}_i$  can be partitioned into subset variable  
 280  $x_a$ , and complement vector  $\mathbf{x}_b$  as follows

$$\mathbf{x}_i = \begin{bmatrix} x_a \\ \mathbf{x}_b \end{bmatrix} \text{ with dimensions } \begin{bmatrix} 1 \times 1 \\ (k-1) \times 1 \end{bmatrix}, \quad (11)$$

281 where  $a = 1, \dots, k$  and  $\mathbf{b} = \{1, 2, \dots, k\}$  where  $a \notin \mathbf{b}$ . This partitioning  
 282 allows us to define block-wise mean and covariance as follows:

$$\boldsymbol{\mu} = \begin{bmatrix} \mu_a \\ \boldsymbol{\mu}_{\mathbf{b}} \end{bmatrix} \text{ with dimensions } \begin{bmatrix} 1 \times 1 \\ (k-1) \times 1 \end{bmatrix}, \quad (12)$$

283 and

$$\boldsymbol{\Sigma} = \begin{bmatrix} \sigma_{aa}^2 & \boldsymbol{\Sigma}_{ab} \\ \boldsymbol{\Sigma}_{ba} & \boldsymbol{\Sigma}_{bb} \end{bmatrix} \text{ with dimensions } \begin{bmatrix} 1 \times 1 & 1 \times (k-1) \\ (k-1) \times 1 & (k-1) \times (k-1) \end{bmatrix}. \quad (13)$$

284 Subsequently, we can derive the conditional distribution of any subset  
 285 variable  $x_a$ , given the complementary vector  $\mathbf{x}_b$ . This conditional distribution  
 286 conforms to a univariate normal distribution, characterized by:

$$X_a | \mathbf{X}_b \sim \mathcal{N}(\mu_{a|\mathbf{b}}, \sigma_{a|\mathbf{b}}^2). \quad (14)$$

287 where  $\mu_{a|\mathbf{b}}$  denotes the conditional mean and  $\sigma_{a|\mathbf{b}}^2$  represents the conditional variance.  
 288 These crucial parameters can be computed by applying the Schur complement as follows:  
 289

$$\sigma_{a|\mathbf{b}}^2 = \sigma_{aa}^2 - \boldsymbol{\Sigma}_{ab}\boldsymbol{\Sigma}_{bb}^{-1}\boldsymbol{\Sigma}_{ba}, \quad (15)$$

290 for the conditional variance  $\sigma_{a|\mathbf{b}}^2$ , while the conditional mean, denoted as  
 291  $\mu_{a|\mathbf{b}}$ , is determined by:

$$\mu_{a|\mathbf{b}} = \mu_a + \boldsymbol{\Sigma}_{ab}\boldsymbol{\Sigma}_{bb}^{-1}(\mathbf{x}_b - \boldsymbol{\mu}_b). \quad (16)$$

292 The conditional variance  $\sigma_{a|\mathbf{b}}^2$  essentially represents the Schur complement  
 293 of  $\boldsymbol{\Sigma}_{bb}$  within the overall covariance matrix  $\boldsymbol{\Sigma}$ .

### 294 2.5. Gaussian Anomaly Detection

295 From a viewpoint of statistics, outliers are commonly denoted as values  
 296 that significantly deviate from the mean. Under the assumption that the  
 297 spatial and temporal characteristics of a system, observed over a moving  
 298 window, can be suitably represented as normally distributed features, we  
 299 assert that any anomaly can be identified as an outlier.

300 In empirical fields like machine learning, the three-sigma rule ( $3\sigma$ ) provides  
 301 a framework for characterizing the region of a distribution within which  
 302 normal values are expected to fall with high confidence. This rule renders  
 303 approximately 0.265% of values in the distribution as anomalous.

304     The  $3\sigma$  rule establishes the probability that any sample  $x_a$  of a random  
 305     vector  $X$  falls within a given CDF over a semi-closed interval as the distance  
 306     from the conditional mean  $\mu_{a|\mathbf{b}}$  of 3 conditional variances  $\sigma_{a|\mathbf{b}}^2$  and gives an  
 307     approximate value of  $q$  as

$$q = P\{|x_a - \mu_{a|\mathbf{b}}| < 3\sigma_{a|\mathbf{b}}^2\} = 0.99735. \quad (17)$$

308     Utilizing a probabilistic model of normal behavior, we can determine  
 309     threshold values  $x_l$  and  $x_u$  corresponding to the closed interval of the CDF  
 310     where this probability is established. The inversion of Equation (10) facili-  
 311     tates this calculation, yielding:

$$x_l = F((1 - P\{|x_a - \mu_{a|\mathbf{b}}| < 3\sigma_{a|\mathbf{b}}^2\}); \mu_{a|\mathbf{b}}, \sigma_{a|\mathbf{b}}^2)^{-1}, \quad (18)$$

312     for the lower limit, and

$$x_u = F((P\{|x_a - \mu_{a|\mathbf{b}}| < 3\sigma_{a|\mathbf{b}}^2\}); \mu_{a|\mathbf{b}}, \sigma_{a|\mathbf{b}}^2)^{-1}, \quad (19)$$

313     for the upper limit. These lower and upper limits together form vectors  
 314      $\mathbf{x}_l$  and  $\mathbf{x}_u$ , respectively, defining the region of normal system operation. This  
 315     region is conceptualized as a hypercube in the feature space, with each di-  
 316     mension bounded by the corresponding feature limits, as computed using  
 317     Equations (18) and (19) for all  $a = 1, \dots, k$ ;  $\mathbf{b} = \{1, 2, \dots, k\}$  where  $a \notin \mathbf{b}$ .  
 318     The approximation of a confidence ellipse as a hypercube can be employed  
 319     to represent the region of normal system operation for individual variables  
 320     of a multivariate system, rendering it as an aid for visual representation.

321     The predicted state of the system, denoted as  $y_i$ , and the normality of  
 322     signals  $\mathbf{y}_{s,i}$  at time  $i$  are determined based on the maximum distance of  
 323     observations from the center of the probabilistic density. The center of the  
 324     probabilistic density corresponds to the vector of conditional means  $\mu_{a|\mathbf{b}}$  with  
 325     respect to other features. The calculation of this distance involves the cumu-  
 326     lative distribution function (CDF) of observations and conditional distribu-  
 327     tions, as follows:

$$F(x_a; \mu_{a|\mathbf{b}}, \sigma_{a|\mathbf{b}}^2) : a = 1, \dots, k; \mathbf{b} = \{1, 2, \dots, k\} \text{ where } a \notin \mathbf{b}. \quad (20)$$

328     Subsequently, operation states of individual inputs are defined as follows:

$$\mathbf{y}_{s,i} = \begin{cases} 0 & \text{if } T \leq (20) \\ 1 & \text{if } T > (20), \end{cases} \quad (21)$$

329 where  $T$  represents a threshold that distinguishes between normal signal  
330 measurement ( $\mathbf{y}_{s,i} = 0$ ) and abnormal ( $\mathbf{y}_{s,i} = 1$ ).

331 For the overall abnormality of the system, any anomaly in signals  $\mathbf{y}_{s,i}$  is  
332 considered, resulting in:

$$y_i = \begin{cases} 1 & \text{if } 1 \in \mathbf{y}_{s,i} \\ 0 & \text{otherwise,} \end{cases} \quad (22)$$

333 defining the discrimination boundary between system operation where  
334  $y_i = 0$  indicates normal system operation, and  $y_i = 1$  indicates anomalous  
335 operation.

### 336 2.6. Anomaly Definition

337 This subsection provides an overview of the definition of anomalies in  
338 data analysis and their categorization, setting conventions for this paper.

339 In the realm of data analysis, anomalies are conspicuous deviations from  
340 the anticipated patterns within a dataset. Traditionally, the task of anomaly  
341 detection has relied upon unsupervised methodologies, wherein the identifi-  
342 cation of "outliers" entails the comparison of data points in both temporal  
343 and spatial contexts. This approach, often referred to as point-wise anomaly  
344 detection, classifies a data point as an anomaly when it exhibits significant  
345 dissimilarity from its neighboring data points (Iglesias Vázquez et al., 2023).

346 The concept of point anomalies, influenced by factors such as temporal  
347 and spatial aspects, can be further categorized into conditional and contex-  
348 tual anomalies (Ruff et al., 2021).

349 Nevertheless, this conventional method may not be suitable for scenarios  
350 characterized by collective anomalies, where clusters of abnormal data points  
351 coexist. A more pragmatic approach defines anomalies as deviations from  
352 established "normal" patterns, resembling the principles of semi-supervised  
353 learning. Change point detection, in a similar vein, can be regarded as a  
354 relative approach that takes into account the varying dynamics of changes,  
355 whether they occur gradually or abruptly (Iglesias Vázquez et al., 2023).

356 It is imperative to recognize that the interpretation of anomalies, outliers,  
357 and novelties can vary upon the application. Anomalies typically garner  
358 significant attention, while outliers are often treated as undesirable noise  
359 and are typically excluded during data preprocessing. Novelties, on the other  
360 hand, signify new observations that necessitate model updates to adapt to  
361 an evolving environment (Ruff et al., 2021).

362        Notwithstanding the differences in terminology, methods employed for the  
363   identification of data points residing in low-probability regions, irrespective of  
364   whether they are referred to as "anomaly detection," "outlier detection," or  
365   "novelty detection," share fundamental similarities (Iglesias Vázquez et al.,  
366   2023).

367 **3. Adaptive Anomaly Detection and Interpretation Framework**

368 In this section, we present an adaptive and interpretable detection frame-  
369 work (AID) designed for SCADA-based industrial systems with streaming  
370 IoT devices. Our approach is rooted in the foundational concepts discussed  
371 in Preliminaries 2. We systematically leverage these theoretical building  
372 blocks to introduce our method in a coherent manner.

373 Our approach begins by modeling the system as a dynamic multivariate  
374 normal distribution, allowing it to effectively handle pervasive nonstationary  
375 effects and interactions that impact industrial processes. We address several  
376 critical factors, such as change points, concept drift, and seasonal effects.  
377 Our primary contribution is the integration of an adaptable self-supervised  
378 system with root cause identification and dynamic operating limits setting.  
379 This unique combination empowers our online statistical model to diagnose  
380 anomalies through three distinct mechanisms.

381 Firstly, we employ conditional probability calculations to assess the nor-  
382 mality of the system’s operating conditions. This step ensures that our  
383 method identifies outliers within individual signal measurements and inter-  
384 prets the root causes of anomalies, facilitating faster and more precise diag-  
385 noses. Secondly, we detect abrupt changes due to concept drift, serving for  
386 faster adaptation to new operating conditions without human intervention.  
387 Thirdly, we harness interpretability as a tool to establish dynamic operating  
388 limits. These adaptive limits enable our framework to seamlessly integrate  
389 with existing SCADA-based infrastructure, a substantial advantage over ex-  
390 isting solutions.

391 We have structured the subsequent sections to delve into the details of our  
392 proposed methodology by the logical flow of data. The upcoming subsection  
393 will cover the anomaly detection mechanism, followed by sections on online  
394 training and adaptation. The next subsection will describe dynamic operat-  
395 ing limits setting, followed by diagnostic capabilities. Lastly, we describe how  
396 those parts converge into a diagnostic tool. For a schematic representation of  
397 our proposed method, with a highlighted subsection attribution, please refer  
398 to Figure 2. For a concise technical representation of our proposed method,  
399 please refer to Algorithm 1.

400 *3.1. Online detection*

401 In the online detection phase, AID distinguishes between normal and  
402 anomalous observations based on the model of the system’s normal behavior.

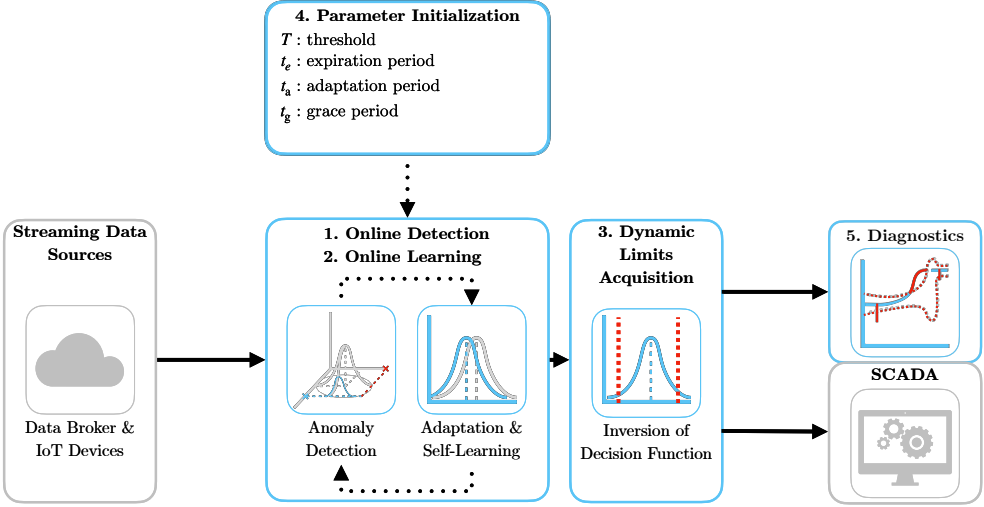


Figure 2: Schematic representation of the proposed method AID with parameter initialization. Colored boxes represent steps described within the subsection.

403 The detection pipeline is event-triggered upon the arrival of a new set of  
 404 measurements.

405 To initiate the process, AID computes the properties of the conditional  
 406 distribution based on the current observations given the dynamic joint nor-  
 407 mal distribution. These calculations are performed for each element of the  
 408 process observation vector  $\mathbf{x}_i$  at time instance  $i$ . Specifically, we calculate the  
 409 conditional mean using (16) and the conditional variance using (15) for ele-  
 410 ments of  $\mathbf{x}_i$ . These computations yield univariate conditional distributions  
 411 for individual signals and features. These conditional distributions play a  
 412 crucial role in assessing the abnormality of signals and features concerning  
 413 their relationships with other elements of  $\mathbf{x}_i$ . Consequently, AID inherently  
 414 considers the interactions between input signals and features.

415 The determination of anomalous behavior is influenced by the parame-  
 416 ter  $T$ , which is a user-defined hyperparameter representing a probabilistic  
 417 threshold that sets the boundary between normal and anomalous behavior.  
 418 Details regarding the selection of an appropriate value for  $T$  are discussed  
 419 in Subsection 3.5. Whenever an anomaly is detected within one of the sig-  
 420 nals or features, it triggers an alert regarding the overall system's anomalous  
 421 behavior, as described in (22). Nevertheless, individual determinations of

422 anomalies serve as a diagnostic tool for isolating the root causes of anomalies,  
423 as further discussed in Subsection 3.4.

424 The proposed mechanism is applicable to both point anomalies and collective  
425 anomalies. In the case of collective anomalies, their duration and deviation  
426 may serve as precursors to concept drift in the system. To identify concept drift,  
427 we introduce a parameter adaptation period  $t_a$ . Given the predicted system anomaly  
428 state from (22) as  $y_i$  over a window of past observations  $\mathbf{y}_i = \{y_{i-t_a}, \dots, y_i\}$  bounded by  $t_a$ ,  
429 the following test determines anticipated change points:  
430

$$\frac{\sum_{y \in \mathbf{y}_i} y}{n(\mathbf{y}_i)} > T. \quad (23)$$

431 Here,  $n(\mathbf{y}_i)$  denotes the dimensionality of  $\mathbf{y}_i$ . The logic behind (23) is  
432 that over an adaptation period  $t_a$ , change points can be distinguished from  
433 collective anomalies and point anomalies due to their minimum duration,  
434 while  $T$  allows for some overlap with previous normal conditions.

435 Our framework anticipates unexpected novel behavior, including non-uniformities  
436 in sampling. Assuming that the distribution of sampling times  
437 remains stable over the long term, we can employ equivalent steps on the  
438 observed time between samples to discriminate signal loss from long-term  
439 anomalous network events.

### 440 3.2. Online learning

441 AID's training process follows an incremental self-learning approach, allowing  
442 for online model updates as new samples arrive. Self-learning, in this  
443 context, focuses on selecting only relevant data for training to maintain the  
444 model's long-term relevancy and stability. This approach proves particularly  
445 valuable in handling streaming data, where human supervision can introduce  
446 significant computational delays, affecting response time in a sequential  
447 setting.

448 In online anomaly detector training, regardless of the type of supervision,  
449 the learning is typically built upon observations of the normal state.  
450 We introduce a grace period denoted as  $t_g$  to enable model calibration in  
451 the initial stages after deployment. During this period, when normality in  
452 samples is expected, the model learns from all observations. Subsequently,  
453 self-supervised and unsupervised detectors are expected to make autonomous  
454 decisions.

455     However, in the case of industrial systems, the drifts in the concept might  
456     often render the normal state anomalous, slowing down or preventing adap-  
457     tation completely. This is particularly true for the case of seasonal effects,  
458     where the system is expected to operate in a different mode for a certain  
459     period of time. To address this issue, AID’s adaptation incorporates two  
460     self-supervised mechanisms.

461     Firstly, the model is updated if the observation at time instance  $i$  is  
462     marked normal in the detection phase. In the case of a dynamic multivariate  
463     probability distribution, the updated parameters are  $\mu_i$  and  $\Sigma_i$  at time in-  
464     stance  $i$ . Update of the mean vector  $\mu_i$  and covariance matrix  $\Sigma_i$  is governed  
465     by Welford’s online algorithm using equation (2) and (4) respectively. Sam-  
466     ples beyond the expiration period  $t_e$ , discussed further in Subsection 3.5, are  
467     disregarded during the second pass. The effect of expired samples is reverted  
468     using inverse Welford’s algorithm for mean (6) and variance (7), accessing  
469     the data in the bounded internal buffer. For more details, refer to Subsection  
470     2.2.

471     The second mechanism, which enables adaptation to anomalous samples,  
472     relies on changepoint detection. This mechanism operates under the as-  
473     sumption that detected changepoints represent new operational states with  
474     limited overlap with the previous ones, as specified in Equation 23. It facili-  
475     tates rapid adaptation to evolving data patterns without the need for human  
476     intervention. The selection of the adaptation period  $t_a$ , as discussed further  
477     in Subsection 3.5, is thus crucial for determining the speed of adaptation or  
478     the potential mitigation of the second adaptation mechanism.

479     To anticipate potential deviations from sampling uniformity, we calculate  
480     the cumulative distribution function (CDF) over the univariate normal dis-  
481     tribution of sampling. We operate under the assumption that, over the long  
482     term, the distribution of sampling times remains stable, employing a one-  
483     pass update mechanism of (2) and (4), for efficiency. To proactively detect  
484     subtle changes in sampling patterns, self-supervised learning is employed,  
485     leveraging anomalies weighted by the deviation from  $(1 - F(x_i; \mu, \sigma^2))$  for  
486     training.

487     3.3. *Dynamic limits acquisition*

488     As we wrote in the subsection Practical Impact 1.4, the monitoring mech-  
489     anisms of SCADA readily depend on the upper and lower operating limits  
490     of individual parameters of the system. In the case of industrial systems,

491 these limits are often defined by the sensor’s designed limits and the sys-  
492 tem dynamics. These limits are typically static and do not account for the  
493 dynamically changing conditions. Our proposed method AID is capable of  
494 setting dynamic operating limits, thus allowing integration into the existing  
495 SCADA-based infrastructure.

496 The threshold  $T$  applied on the dynamic multivariate normal distribution  
497 creates a confidence hyperellipse at  $T$  probability level. Such a hyperellipse  
498 would not allow to effectively bound individual signals as it depends on val-  
499 ues that other jointly distributed variables take. Nevertheless, by computing  
500 the conditional for process observation vector  $\mathbf{x}_i$  at time instance  $i$ , we can  
501 compute the conditional density function for individual signals. By applying  
502 threshold  $T$  on individual conditional probabilities, we establish a hyper-  
503 cube defined by lower and upper threshold values, denoted as  $\mathbf{x}_l$  and  $\mathbf{x}_u$ ,  
504 respectively. These thresholds are derived from (18) and (19), incorporating  
505 updated model parameters. Lower and upper thresholds play a pivotal role  
506 as dynamic operating limits. They may be used as an addition to static op-  
507 erating limits used by monitoring systems in SCADA, accounting for spatial  
508 factors, such as multipoint measurements, temporal factors, such as aging,  
509 and actual environmental conditions that influence sensor operation. More-  
510 over, any violation of the limits is also detected as an anomaly.

511 *3.4. Diagnostics*

512 One of the crucial aspects of diagnostics is root cause isolation. Using the  
513 ability to detect anomalies in individual signals and features, AID is capable  
514 of isolating the root cause of anomalies with consideration of their mutual  
515 relationships. This is achieved by computing the conditional probability of  
516 individual signals and features given the rest of the process observation vec-  
517 tor  $\mathbf{x}_i$  at time instance  $i$ . The dynamic process limits further enhance the  
518 diagnosis by providing the context of the anomaly, including the extent of  
519 deviation from normal operation and the direction of the deviation. The  
520 proposed diagnostic mechanism is particularly useful in the case of collec-  
521 tive anomalies, where the unified direction of deviations is expected. AID’s  
522 interpretability is an asset for domain experts to understand why certain  
523 anomalies are flagged and enables operators to assess the system’s state by  
524 visualizing limits and deviations, thus detecting the speed at which the pro-  
cess variable approaches the limits before an anomaly occurs.

526    3.5. Model Parameters Initialization

527    The model initialization is governed by defining two required hyperparameters of the model: the expiration period ( $t_e$ ) and the threshold ( $T$ ). The  
528 expiration period determines the window size for time-rolling computations,  
529 impacting the proportion of outliers within a given timeframe and directly in-  
530 fluencing the relaxation (with a longer expiration period) or tightening (with  
531 a shorter expiration period) of dynamic signal limits. Additionally, we intro-  
532 duce a grace period  $t_g$ , which defaults to  $uite$ , allowing for model calibration.  
533 During this grace period, system anomalies are not flagged to prevent false  
534 positives and speed up self-supervised learning, introduced in Subsection 3.2.  
535  $t_g$  can take any value smaller than  $uite$ , if the detection must be delivered fast  
536 after intergration. The length of the expiration period inversely correlates  
537 with the model’s ability to adapt to sudden changes. The adaptation and  
538 detection of significant drifts in the data-generating process, such as changes  
539 in central tendency, is managed through the adaptation period  $t_a$ . A shorter  
540  $t_a$  results in faster adaptation to new operating conditions, while making the  
541 system vulnerable to prolonged collective anomalies. A longer  $t_a$  results in  
542 slower adaptation to significantly deviating new operations, but allows longer  
543 alerts regarding collective anomalies. In most cases,  $t_a = 1/4t_e$  offers optimal  
544 performance.

545    As a general rule of thumb, expiration period  $t_e$  should be determined  
546 based on the slowest observed dynamics within the multivariate system. The  
547 threshold  $T$  defaults to the three-sigma probability of  $q$  in (17). Adjusting  
548 this threshold can fine-tune the trade-off between precision and recall. A  
549 lower threshold boosts recall but may lower precision, while a higher thresh-  
550 old enhances precision at the cost of recall. We recommend starting with  
551 the default values of other parameters and making adjustments based on  
552 real-time model performance, as the model’s interpretability can reduce the  
553 time and effort required for fine-tuning. The presence of one non-default  
554 interpretable hyperparameter facilitates quick adaptation of AID in a broad  
555 range of use cases.

---

**Algorithm 1** Online Detection and Identification Workflow

---

**Input:** expiration period  $t_e$

**Output:** system anomaly  $y_i$ , signal anomalies  $\mathbf{y}_{s,i}$ , sampling anomaly  $y_{t,i}$ , change-point  $y_{c,i}$ , lower thresholds  $\mathbf{x}_{l,i}$ , upper thresholds  $\mathbf{x}_{u,i}$ ,

*Initialisation :*

- 1:  $i \leftarrow 1; n \leftarrow 1; T \leftarrow (17); \boldsymbol{\mu} \leftarrow \mathbf{x}_0; \boldsymbol{\Sigma} \leftarrow \mathbf{1}_{k \times k}; \mu_t \leftarrow 0; \sigma_t^2 \leftarrow 1;$
  - 2: compute  $F(\mathbf{x}_0; \boldsymbol{\mu}, \boldsymbol{\Sigma})$  using algorithm in Genz (2000);  
*LOOP Process*
  - 3: **loop**
  - 4:    $\mathbf{x}_i, t_i \leftarrow \text{RECEIVE}();$
  - 5:    $\mathbf{y}_{s,i} \leftarrow \text{PREDICT}(\mathbf{x}_i, T)$  using (21);
  - 6:    $y_i \leftarrow \text{PREDICT}(\mathbf{y}_{s,i})$  using (22);
  - 7:    $\mathbf{x}_{l,i}, \mathbf{x}_{u,i} \leftarrow \text{GET}(T, \boldsymbol{\mu}, \boldsymbol{\Sigma})$  using (18), (19);
  - 8:    $y_{t,i} \leftarrow \text{PREDICT}(t_i - t_{i-1})$  using (21);
  - 9:    $\mu_t, \sigma_t^2 \leftarrow \text{UPDATE}(t_i - t_{i-1}, \mu_t, \sigma_t^2)$  using (2), (4);
  - 10:   **if** (22) = 0 **or** (23) **then**
  - 11:      $\boldsymbol{\mu}, \boldsymbol{\Sigma} \leftarrow \text{UPDATE}(\mathbf{x}_i, \boldsymbol{\mu}, \boldsymbol{\Sigma}, n)$  using (2), (4);
  - 12:     **if** (23) **then**
  - 13:        $y_{c,i} \leftarrow 1;$
  - 14:     **else**
  - 15:        $y_{c,i} \leftarrow 0;$
  - 16:     **end if**
  - 17:      $n \leftarrow n + 1;$
  - 18:     **for**  $\mathbf{x}_{i-t_e}$  **do**
  - 19:        $\boldsymbol{\mu}, \boldsymbol{\Sigma} \leftarrow \text{REVERT}(\mathbf{x}_{i-t_e}, \boldsymbol{\mu}, \boldsymbol{\Sigma}, n)$  using (6), (7);
  - 20:        $n \leftarrow n - 1;$
  - 21:     **end for**
  - 22:   **end if**
  - 23:    $i \leftarrow i + 1;$
  - 24: **end loop**
-

557    **4. Case Study**

558    This section presents two case studies on real industrial-scale energy stor-  
559    ages and a real data benchmark to demonstrate the effectiveness and appli-  
560    cability of our proposed approach. We investigate the properties and perfor-  
561    mance of the approach using signals from IoT devices in an energy system  
562    and streamed benchmark system data. The successful deployment demon-  
563    strates that this approach is suitable for existing industrial systems utilizing  
564    IoT data streams on top of well-established SCADA systems.

565    *4.1. Battery Energy Storage System TERRA*

566    In the first case study, we demonstrate our proposed method on real  
567    industrial-scale battery energy storage system (BESS) TERRA, depicted in  
568    Fig 3. TERRA has an installed capacity of 151 kWh distributed among  
569    10 modules with 20 cells. The Inverter's nominal power is 100 kW. The  
570    TERRA reports measurements of State of Charge (SoC), supply/draw energy  
571    set-points, and inner temperature, at 6 positions (channels) of each battery  
572    module. A substantial size of the system, which is 2.4x2.4x1.2m (HxWxD),  
573    requires a proper cooling mechanism. The cooling is handled by forced air  
574    from the HVAC system and inner fans, while the fire safety system is passive.  
575    Tight battery temperature control is needed to optimize performance and  
576    maximize the safety and battery's lifespan. Identifying anomalous events  
577    and removal of corrupted data might yield significant improvement in the  
578    process control level and increase the reliability and stability of the system.

579    The AID is integrated into the existing software infrastructure of the  
580    system, allowing detection and diagnosis of the system using streamed IoT  
581    data. Here we replay a 9-day stream of historical measurements of the device,  
582    to demonstrate key features of AID.

583    For demonstration purposes, the expiration period  $t_e$  is set to 4 days, as  
584    the system is expected to adapt to the new behavior, due to the transfer of  
585    the module to the outside. The grace period was reduced to 1 day, to observe  
586    the reaction to concept drift. The threshold  $T$  is set to  $3.5\sigma$  to reduce the  
587    number of alarms. The frequency will be higher as the detector is protected  
588    and self-supervised. The adaptation period  $t_a$  is changed to 3 hours as this  
589    is the time constant of the temperature to the unit change of supply/draw  
590    power demand.

591    Figure 4 depicts the average cell temperature measurement of the TERRA  
592    for all 10 modules. The data are normalized to the range [0, 1] to protect



Figure 3: Photograph of the actual studied TERRA energy storage unit with open doors (left), and closed doors (right).

593 the sensitive business value. The light red area represents the region out of  
 594 dynamic operating limits as provided by AID. On 7<sup>th</sup> March 2022, the system  
 595 was relocated from the inside of the building to the outside power socket. The  
 596 system was expected to adapt to the new behavior within 4 days as specified  
 597 by  $t_e$ . Nevertheless, due to the protection of the model from learning the  
 598 anomalous data, the new behavior could not be captured as the system was  
 599 not operating within the safe limits. The adaptation started three days later,  
 600 as only some of the measurements within the safe region after transfer were  
 601 learned. Therefore, the importance of self-supervised adaptation to changes  
 602 in data is crucial. As we can see, the change points detection according to  
 603 (??) alerted such change shortly after the TERRA was connected to a data  
 604 broker, while the length of the adaptation period enabled discrimination from  
 605 collective anomaly.

606 In Figure 5 we depict the same measurement with a changepoint adap-  
 607 tation mechanism in place. The mechanism speeds up the adaptation to the  
 608 new behavior, as the system is allowed to learn from anomalous data when  
 609 they represent the changed behavior. The adaptation took approximately 6  
 610 times shorter.

611 The default sampling rate of the incoming signal measurements is 1  
 612 minute. However, network communication of the IoT devices is prone to  
 613 packet dropout, which results in unexpected non-uniformities in sampling  
 614 from the perspective of the SCADA system. The transfer of TERRA was

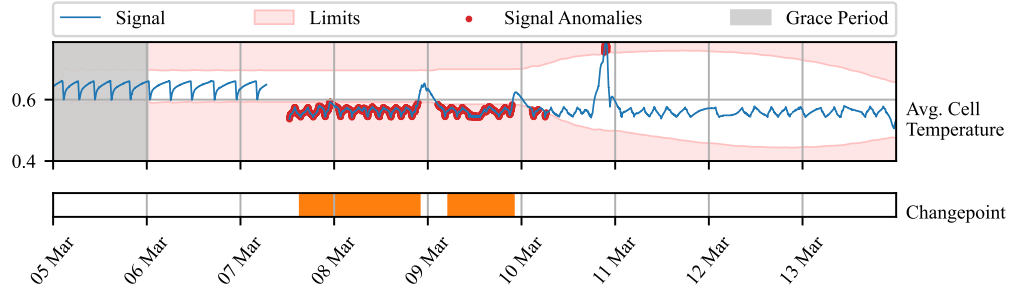


Figure 4: Time series of TERRA measurements observed over 9 days (blue line). The y-axis renders the average temperature of all cells and modules after the normalization to the range of [0, 1]. The light red area represents an area out of dynamic operating limits for individual signals. Observations out of the limits are marked by a red dot. Orange bars represent the times, at which changepoints were detected. Grace period is grayed out.

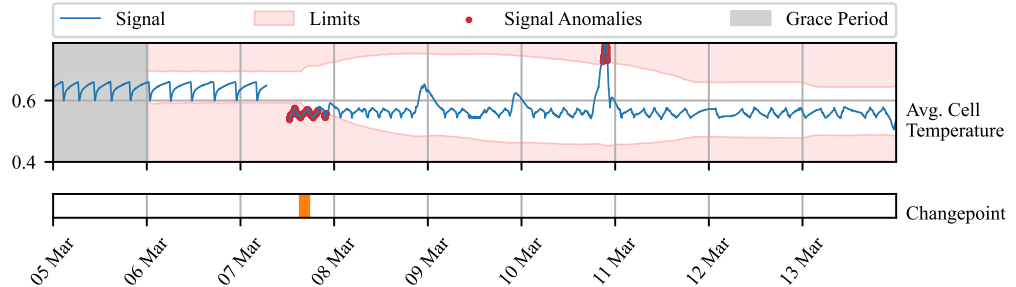


Figure 5: Time series of TERRA measurements observed over 9 days (blue line). The y-axis renders the average temperature of all cells and modules after the normalization to the range of [0, 1]. The light red area represents an area out of dynamic operating limits for individual signals. Observations out of the limits are marked by a red dot. Orange bars represent the times, at which changepoints were detected. Grace period is grayed out.

615 accompanied by the disconnection of IoT sensors from the data broker which  
 616 might be considered an anomaly. The system can detect such anomalies as  
 617 well, as depicted in Figure 6. Along with known disconnection, the system  
 618 alerted two more non-uniformities of shorter extend, scaled in the figure for  
 619 better visibility. The short loss of signal was caused by the packet drop, as  
 620 it impacted only a few consecutive measurements. Various confidence levels  
 621 could be used to further analyze and map potential causes to the duration  
 622 of the outage.

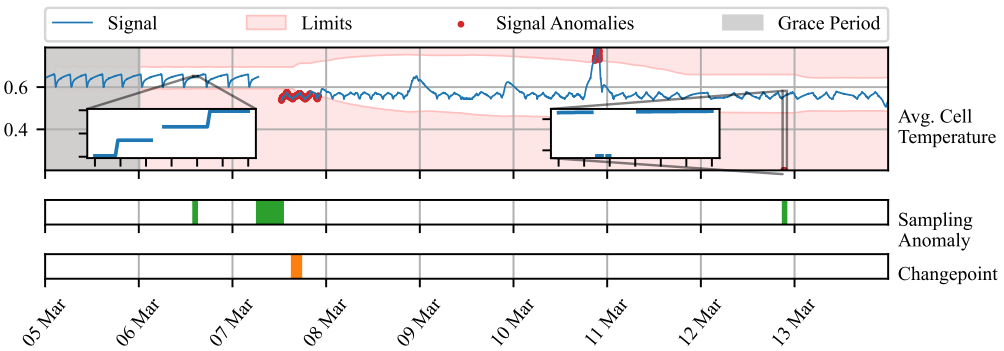


Figure 6: Time series of TERRA measurements observed over 9 days (blue line). The y-axis renders the average temperature of all cells and modules after the normalization to the range of [0, 1]. The light red area represents an area out of dynamic operating limits for individual signals. Observations out of the limits are marked by a red dot. Orange bars represent the times, at which changepoints were detected. Green bars represent periods where sampling anomaly was alerted. Grace period is grayed out.

623 Lastly, we want to acknowledge the outlier, left uncaptured due to in-  
 624 creased variance of the distribution in a period of adaptation. Observing  
 625 multiple variables, where some might be influenced less by the change in be-  
 626 havior, might be beneficial in such cases. The industrial partner provided a  
 627 physics-based model of the battery module temperature, defined as follows:

$$\begin{aligned}
 T_{\text{bat},i+1} = & T_{\text{bat},i} + T_s(q_{\text{fan}} V_{\text{b,max}} \rho c_p (T_{\text{out}} - T_{\text{bat},i}) + V_{\text{c,max}} q_{\text{circ,fan}} \rho c_p T_{\text{bat},i} \\
 & + q_{\text{circ,fan}} (P_{\text{cool}} q_{\text{cool}} P_{\text{heat}} q_{\text{heat}}) + c_{\text{scale}} Q_{\text{bat}} + q_{\text{inner fans}} \\
 & - (V_{\text{b,max}} q_{\text{fan}} V_{\text{c,max}} q_{\text{circ,fan}}) \rho c_p T_{\text{bat},i}) / (m_{\text{bat}} c_{\text{p,b}})
 \end{aligned} \tag{24}$$

628 When combined with an averaged measurement of battery module tem-  
 629 perature, we could compute the difference between real and predicted tem-  
 630 perature. Such deviation can be useful in detecting unexpected patterns in

631 temperature due to the impact of external disturbance and aging. Nevertheless,  
632 it may be inaccurate as the physics-based model is simplified and does  
633 not account for spatial aspects, like temperature gradients as well as different  
634 dynamic effects of charging and discharging on temperature. For instance,  
635 in Fig. 3 during the first two days we see, that the cooling dynamic is not  
636 captured well, resulting in a subtle positive difference between average cell  
637 temperature and the temperature predicted by the model. In combination  
638 with the raw measured average of the temperature, the AID captures the  
639 outlier on 9<sup>th</sup> March which could not be captured in a univariate setting.  
640 The physics-based model exposes temporal aspects of the behavior as it con-  
641 siders the dynamics of its inputs. The rapid increase in temperature w.r.t  
642 the modeled dynamics due to environmental conditions will draw a sharp  
643 positive peak in the difference between the real and predicted temperature,  
644 which will slowly vanish. Based on the significance of the deviation, the peak  
645 will be notified as a single-point anomaly or collective anomaly.

646 This case study demonstrated AID’s effectiveness within the context of  
647 the energy storage system, specifically the TERRA system. The AID system  
648 exhibited adaptability to changes in the operational environment, contribut-  
649 ing to its versatility and robustness. Additionally, it facilitated the establish-  
650 ment of dynamic operating limits for SCADA systems, considering context  
651 of the device such as environmental conditions or aging. Furthermore, the  
652 AID system showcased its capability to operate with a physics-based model,  
653 enhancing the precision of anomaly detection processes. This highlights the  
654 potential of AID as a valuable tool within complex industrial systems. The  
655 validity of our proposed approach was verified by our industrial partner, who  
656 confirmed that the detected anomalies were indeed caused by the aforemen-  
657 tioned events.

#### 658 4.2. Kokam Battery Module

659 A second case study presents temperature profile monitoring of individual  
660 modules of battery pack TERRA deployed at the premises of the end user.  
661 During the operation, a hardware fault of module’s 9 cooling fan occurred on  
662 23<sup>rd</sup> August 2023 at 17:12:30. Our industrial partner was interested in find-  
663 ing out, whether such an event could be captured by an anomaly detection  
664 system. Each of the 10 modules, embodies 20 cells measured by 6 spatially  
665 distributed sensors as shown in Figure 8. The measurements are sent in 30-  
666 second intervals and processed in a streamed manner by SCADA. With the  
667 availability of the temperature profiles for all the modules, we computed the

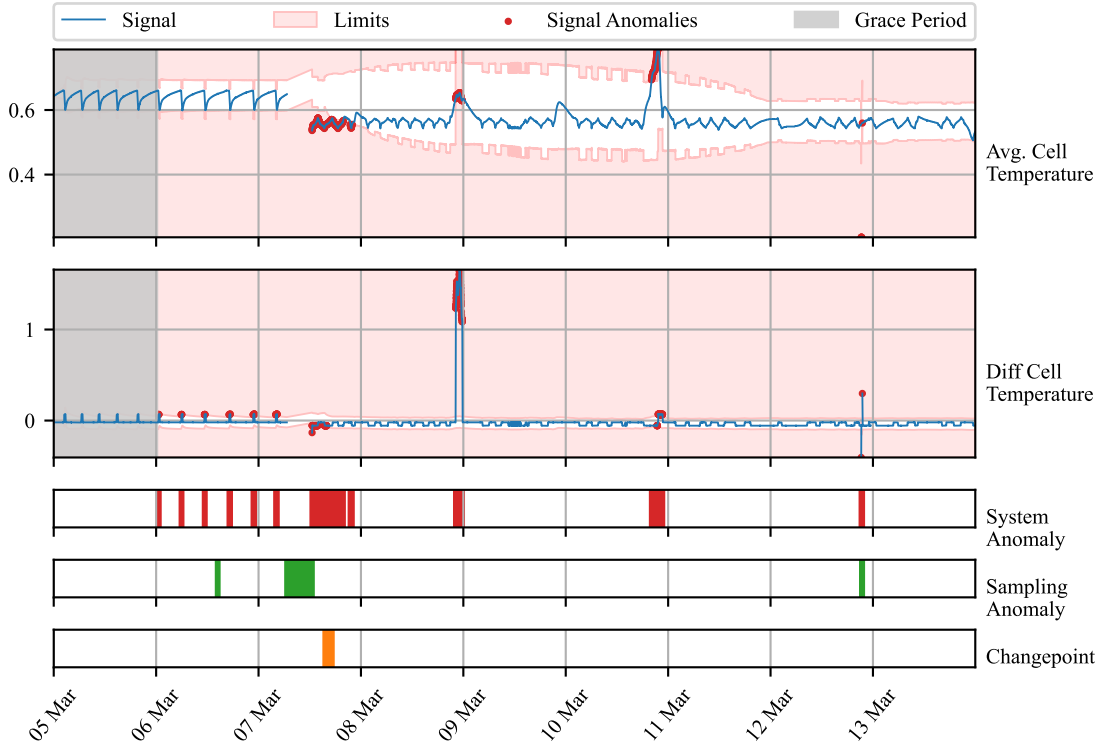


Figure 7: Time series of TERRA measurements observed over 9 days (blue line). The y-axis renders the average temperature of all cells and modules after the normalization to the range of [0, 1]. The light red area represents an area out of dynamic operating limits for individual signals. Observations out of the limits are marked by a red dot. Orange bars represent the times, at which changepoints were detected. Green bars represent periods where sampling anomaly was alerted. Red bars denote the period where any of the signals contained anomaly. Grace period is grayed out.

668 deviation of the observed value from the average of all the modules' temper-  
 669 ature measurements. The ground truth information about the fan fault was  
 670 provided to the best of the operator's knowledge. However, this information  
 671 serves for evaluation only, as the system operates in a self-supervised manner.

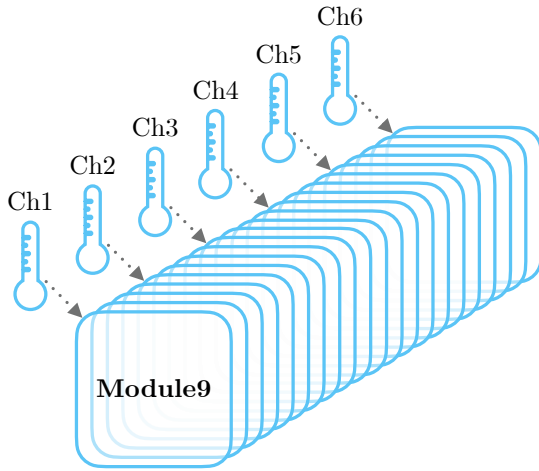


Figure 8: Module 9 with 20 cells and 6 sensors measuring the temperature at each 4<sup>th</sup> cell.

672 Our anomaly detection system was, in this case, initialized for the op-  
 673 eration in production. The expiration period of 7 days, allowed the system  
 674 to adapt to weekly seasonality due to the usage of the battery following  
 675 work week. The grace period was kept at the default value, equal to  $t_e$ . The  
 676 threshold value was shifted to a 4 sigma value of 99.977% which makes the the  
 677 frequency of anomalous events approximately once a week given 30-second  
 678 sampling. The adaptation period was held constant as the deployed system  
 679 is not expected to change its behavior dramatically on a daily basis.

680 In Figure 9 we observe 4 days of operation around the period of fan  
 681 fault occurrence. The deviations between the observed temperature mea-  
 682 sured by channels of module 9 and the average temperature of all modules  
 683 are displayed. The dynamic operating limits tightly envelop temperatures  
 684 measured by the sensors in the middle of the module (refer to Figure 8),  
 685 while measurements at both sides deviate more due to the proximity to the  
 686 walls and sources of disturbance. We observed multiple alarms raised by var-  
 687 ious channels individually before the fan fault. These anomalies, while not

688 addressed here further, could be subjects of interest for further investigation  
689 by system operators. Meanwhile, the fan fault at the center of our focus is  
690 alarmed based on three measurements, namely channels 1, 2, and 3. From  
691 the zoomed views, we can observe a sharp increase in the temperature devia-  
692 tion. The alarm is on until 24<sup>th</sup> August at noon, when significant fluctuations  
693 vanish followed by temporary settling of the temperature. On 25<sup>th</sup> August  
694 at 11:21, increased temperature fluctuations are followed by an increase of  
695 temperature similar to the initial one. AID alerts this fault again based on  
696 measurements by channels 1, 2, and 3.

697 Time series of TERRA measurements observed over 9 days (blue line).  
698 The y-axis renders the average temperature of all cells and modules after the  
699 normalization to the range of [0, 1]. The light red area represents an area out  
700 of dynamic operating limits for individual signals. Observations out of the  
701 limits are marked by a red dot. Orange bars represent the times, at which  
702 changepoints were detected. Green bars represent periods where sampling  
703 anomaly was alerted. Red bars denote the period where any of the signals  
704 contained anomaly. Grace period is grayed out.

705 Interestingly, during the presence of a fault in the fan, two more peri-  
706 ods where the fan started operating again followed as depicted in Figure 10.  
707 Periods of operation were interrupted again on 27<sup>th</sup> and 28<sup>th</sup> August respec-  
708 tively in the early morning hours. In both of the cases, AID detected the  
709 presence of the fault at the moment of occurrence. In the first case, channel  
710 3 reported an anomaly slightly before the increase in temperature, due to  
711 abnormal fluctuation happening prior to faults.

712 This case study demonstrates the effectiveness of the AID framework in  
713 identifying hardware faults within the context of energy storage systems. It  
714 showcases the system’s ability to harness spatially distributed sensors that  
715 measure the same process variable. The AID system successfully pinpointed  
716 a fault in a cooling fan during real-world production operations, underlining  
717 its practical utility and its relevance in enhancing the safety of energy storage  
718 systems. Furthermore, the incorporation of adaptation mechanisms ensures  
719 that the system can be deployed over extended periods without necessitating  
720 resource-intensive retraining. Additionally, the concept of dynamic operating  
721 limits introduced in this study holds promise for integration with Supervisory  
722 Control and Data Acquisition (SCADA) monitoring systems, enabling proac-  
723 tive responses in situations where human life, equipment, or the environment  
724 may be at risk.

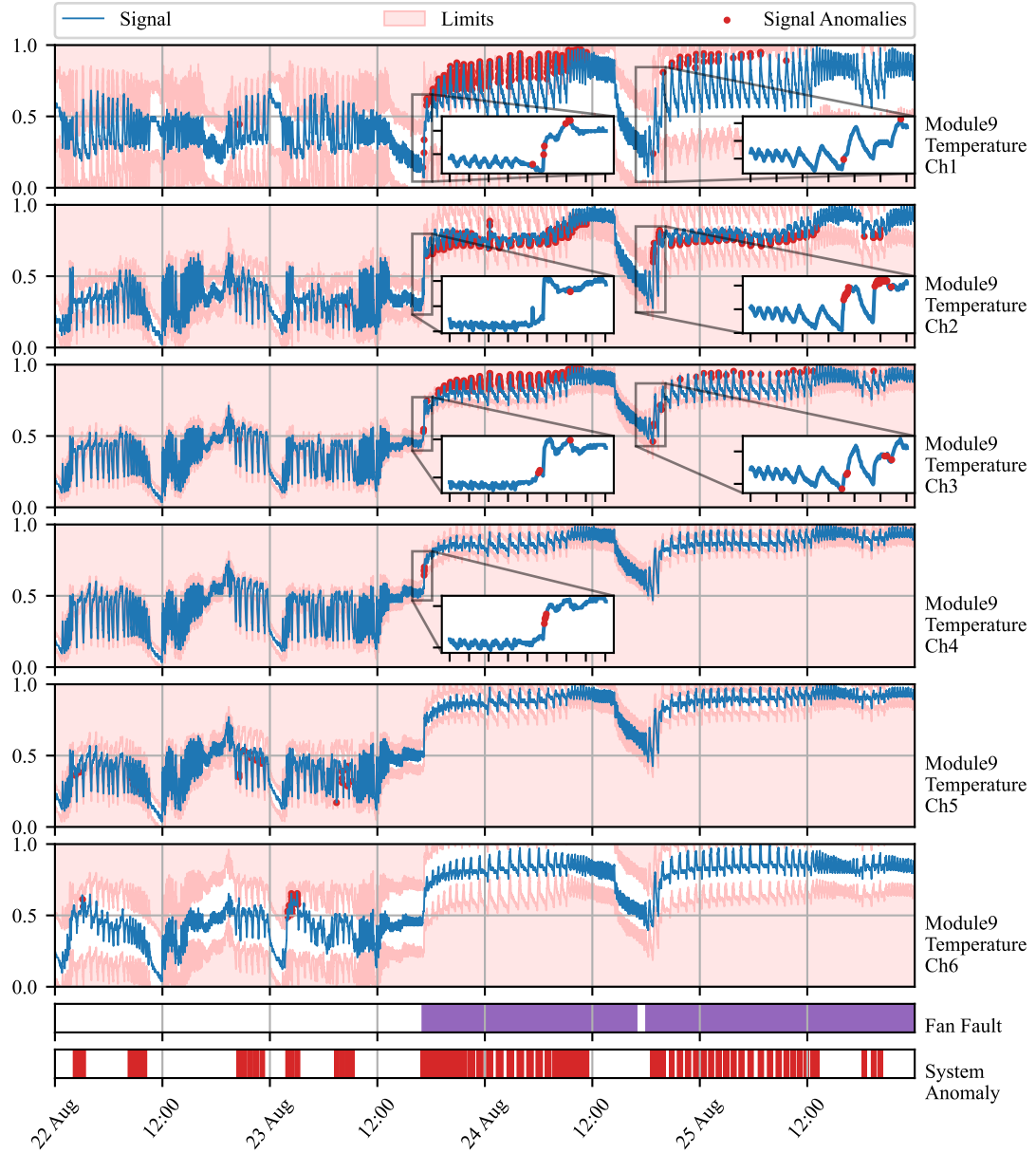


Figure 9: Time series of battery module 9 measurements (blue line). The y-axis renders the normalized deviations of temperature from the average of all modules. Signal anomalies are marked as red dots. The light red area represents an area out of dynamic operating limits. True fan faults are marked by purple bars. Green bars represent the times of changepoint detection. Red bars denote the period where any signal anomaly.

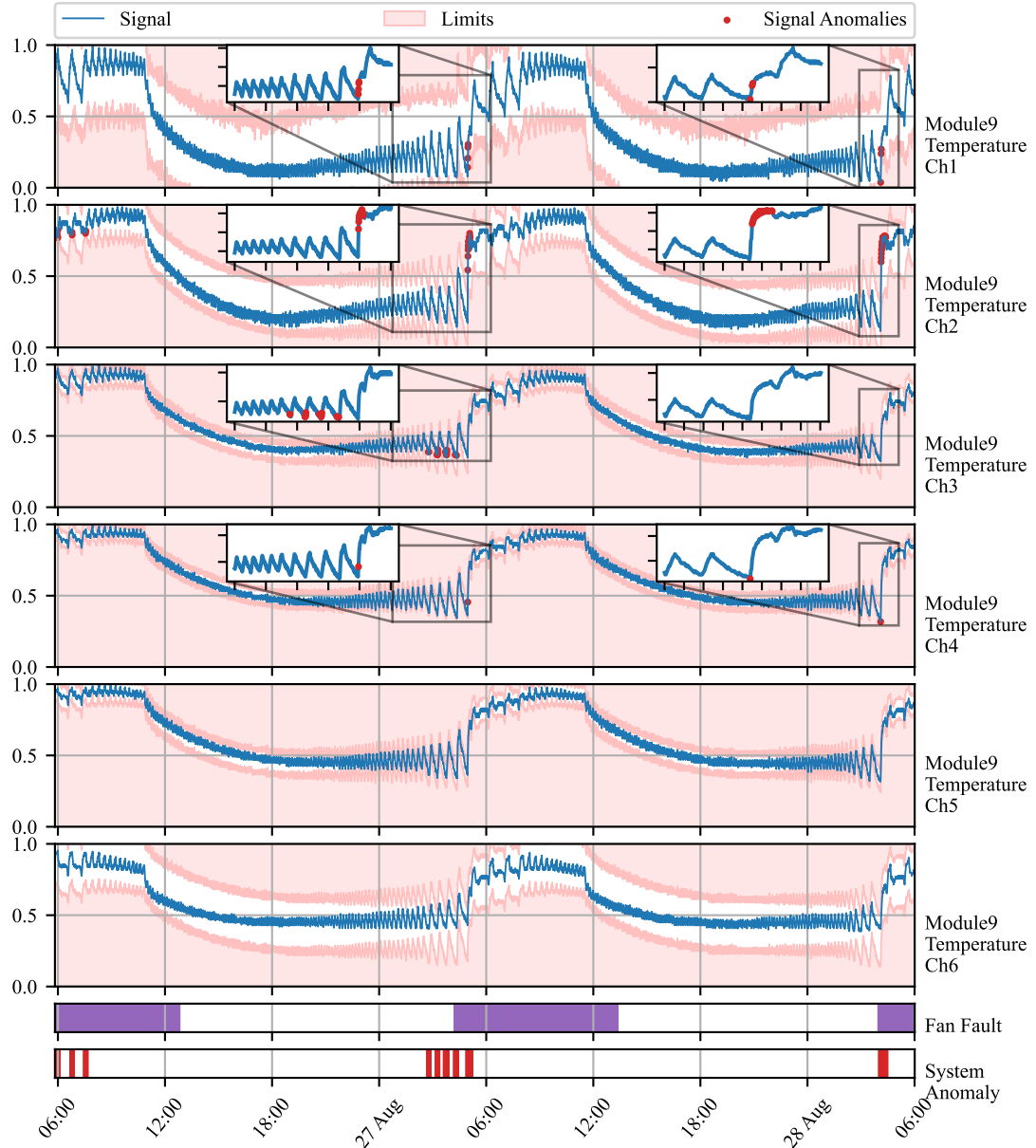


Figure 10: Time series of battery module 9 measurements (blue line). The y-axis renders the normalized deviations of temperature from an average of all modules. Signal anomalies are marked as red dots. The light red area represents an area out of dynamic operating limits. True fan faults are marked by purple bars. Green bars represent the times of changepoint detection. Red bars denote the period where any of the signals contained anomaly.

725     *4.3. Real Data Benchmark*

726     The benchmarking comparison in this subsection evaluates the AID frame-  
727     work against adaptive unsupervised detection methods, specifically One-  
728     Class Support Vector Machine (OC-SVM) and Half-Space Trees (HS-Trees).  
729     These methods are widely recognized for their iterative learning capabilities  
730     on multivariate time-series data, making them suitable for anomaly detection  
731     in dynamic systems, as previously discussed in the Introduction 1.3.

732     The comparison is based on the Skoltech Anomaly Benchmark (SKAB)  
733     dataset, a real-world dataset with annotated labels distinguishing between  
734     anomalous and normal observations (Katser and Kozitsin, 2020). SKAB  
735     is used for this purpose, as no established benchmarking multivariate data  
736     were found regarding energy storage systems similar to the ones studied in  
737     Subsection 4.1 and Subsection 4.2. The SKAB dataset involves experiments  
738     related to rotor imbalance, where various control actions and changes in  
739     water volume are introduced to the system. It encompasses eight features  
740     and exhibits both gradual and sudden drifts.

741     To ensure fairness in the benchmark, data preprocessing adheres to best  
742     practices for each method. OC-SVM employs standard scaling, while HS-  
743     Trees use normalization. Our proposed AID method requires no scaling.  
744     Preprocessing is performed online, simulating a real production environment,  
745     with running mean and variance for standard scaling and running peak-to-  
746     peak distance for normalization, as supported by the online machine learning  
747     library "river" (Montiel et al., 2021).

748     The optimal hyperparameters for both reference methods are found us-  
749     ing Bayesian Optimization. Due to no further knowledge about the data  
750     generating process, and equity in benchmark, the hyperparameters of our  
751     proposed method were optimized using Bayesian Optimization as well. 20  
752     steps of random exploration with 100 iterations of Bayesian Optimization  
753     were used, increasing default values set in the Bayesian Optimization library,  
754     to allow thorough exploration and increase the possibility of finding global  
755     optima in each case (Nogueira, 2014). The hyperparameters are optimized  
756     with the F1 score as a cost function first, to maximize both precision and  
757     recall on anomalous samples.

758     As adaptation is required and anticipated within benchmark datasets,  
759     the performance is evaluated iteratively, similarly to the operation after de-  
760     ployment. The metric is updated with each new sample and its final value is  
761     used to drive Bayesian Optimization. The performance is evaluated using the  
762     best-performing model, found by Bayesian Optimization. The performance

763 of the proposed method is evaluated on the same data as the models are  
764 optimized for.

765 Hyperparameter search ranges are specified, with values centered around  
766 default library values for OC-SVM and HS-Trees. The ranges are intention-  
767 ally set wide to facilitate comprehensive exploration. The quantile filter  
768 threshold used in OC-SVM and HS-Trees aligns with the threshold used in  
769 AID. These hyperparameter ranges are presented in Table 1.

Table 1: Hyperparameter Ranges for Detection Algorithms

Algorithm	Hyperparameters	Default	Ranges
AID	Threshold	0.99735	(0.85, 0.99994)
	$t_e$	-	(150, 10000)
	$t_a$	$t_e$	(50, 2000)
	$t_g$	$t_e$	(50, 1000)
OC-SVM	Threshold	-	(0.85, 0.99994)
	Learning Rate	0.01	(0.005, 0.02)
HS-Trees	Threshold	-	(0.85, 0.99994)
	N Trees	10	(0, 20)
	Max Height	8	(2, 14)
	Window Size	250	(100, 400)

770 The results for models optimized for the F1 score are summarized in Ta-  
771 ble 2, which includes precision, recall, F1 score, and average latency. Macro  
772 values are enclosed in brackets, representing the mean of the metric for both  
773 anomalies and normal data. A perfect detection achieves 100% in each met-  
774 ric. According to the Scoreboard for various algorithms on SKAB’s Kaggle  
775 page, all iterative approaches perform comparably to the batch-trained iso-  
776 lation forest and autoencoder, validating the optimization process. Notably,  
777 the proposed AID method outperforms both reference methods in terms of  
778 F1 score, recall, and precision, despite having a 30-fold higher latency per  
779 sample. This highlights the scalability as a candidate for further develop-  
780 ment. Nevertheless, in this case, sampling of the benchmark data still offers  
781 enough time to deliver predictions with sufficient frequency.

782 Optimal hyperparameters found during Bayesian Optimization are de-  
783 tailed in Table 3. None of the parameters are at the edge of the provided  
784 ranges, serving as necessary proof of ranges being broad enough. Never-  
785 theless, sufficient proof is not possible as multiple parameter ranges are not  
786 bounded by designed limits.

Table 2: Evaluation of models optimized for F1 score on SKAB dataset (Katser and Kozitsin, 2020). The best-performing model is highlighted in bold. Values in brackets represent macro values of the metric.

Algorithm	Precision [%]	Recall [%]	F1 [%]	Avg. Latency [ms]
AID	<b>41</b> (59)	<b>80</b> (59)	<b>54</b> (53)	1.45
HS-Trees	36 (51)	74 (51)	48 (44)	<b>0.05</b>
OC-SVM	39 (54)	63 (54)	48 (52)	<b>0.05</b>

Table 3: Optimal hyperparameters of methods optimized for F1 score

Algorithm	Hyperparameters	Found
AID	Threshold	0.96442
	$t_e$	1136
	$t_a$	396
	$t_g$	546
OC-SVM	Threshold	0.86411
	Learning Rate	0.01956
HS-Trees	Threshold	0.99715
	N Trees	1
	Max Height	7
	Window Size	283

## 787 5. Conclusion

788 In this paper, we demonstrate the capacity of adaptive conditional prob-  
 789 ability distribution to model the normal operation of dynamic systems em-  
 790 ploying streaming IoT data and isolate the root cause of anomalies. AID  
 791 dynamically adapts to non-stationarity by updating multivariate Gaussian  
 792 distribution parameters over time. Additionally, self-supervision enhances  
 793 the model by protecting it from the effects of outliers and increasing the  
 794 speed of adaptation in response to autonomously detected changes in oper-  
 795 ation.

796 Our statistical model isolates the root causes of anomalies as extreme  
 797 deviations from the conditional means vector, considering spatial and tem-  
 798 poral effects encoded in features, as demonstrated in our case studies. This  
 799 approach establishes the system’s operational state by analyzing the dis-

800 tribution of signal measurements, computing the distance from the mean  
801 of conditional probability, and setting dynamic operating limits based on  
802 multivariate distribution parameters. Additionally, the detector alerts for  
803 non-uniform sampling due to packet drops and sensor malfunctions. These  
804 adaptable limits can be seamlessly integrated into SCADA architecture, en-  
805 hancing context awareness and enabling plug-and-play compatibility with  
806 existing infrastructure.

807 The ability to detect and identify anomalies in the system, isolate the  
808 root cause of anomaly to specific signal or feature, and identify signal losses  
809 is shown in two case studies on data from operated industrial-scale energy  
810 storages. These case studies highlight the model’s ability to adapt, diagnose  
811 the root cause of anomalies, and leverage both physics-based models and  
812 spatially distributed sensors. Unlike many anomaly detection approaches,  
813 the proposed AID method does not require historical data or ground truth  
814 information about anomalies, alleviating the general limitations of detection  
815 methods employed in the energy industry.

816 The benchmark performed on industrial data indicates that our model  
817 provides comparable results to other self-learning adaptable anomaly detec-  
818 tion methods. This is an important property of our model, as it also allows  
819 for root cause isolation.

820 AID represents a significant advancement in the safety and profitability  
821 of evolving systems that utilize well-established SCADA architecture and  
822 streaming IoT data. By providing dynamic operating limits, AID seamlessly  
823 integrates with existing alarm mechanisms commonly employed in SCADA  
824 systems. To the best of our knowledge, this study appears to be one of the  
825 initial attempts to introduce a self-supervised approach for adaptive anomaly  
826 detection and root cause isolation in SCADA-based systems utilizing IoT  
827 data streams.

828 Future work on this method will include improvements to the change point  
829 detection mechanism, reduction in latency for high-dimensional data, and  
830 minimizing the false positive rate, which is a challenge for general plug-and-  
831 play models. We will also explore the ability to operate with non-parametric  
832 models, in contrast to Gaussian distribution.

### 833 Additional information

834 Our framework is openly accessible on GitHub at the following URL:  
835 [https://github.com/MarekWadinger/online\\_outlier\\_detection](https://github.com/MarekWadinger/online_outlier_detection).

836 **CRediT authorship contribution statement**

837 **Marek Wadinger:** Conceptualization; Data curation; Formal analysis;  
838 Investigation; Methodology; Resources; Software; Validation; Visualization;  
839 Writing - original draft; and Writing - review & editing. **Michal Kvasnica:**  
840 Conceptualization; Funding acquisition; Project administration; Resources;  
841 Supervision; Validation.

842 **Declaration of Competing Interest**

843 The authors declare that they have no known competing financial inter-  
844 ests or personal relationships that could have appeared to influence the work  
845 reported in this paper.

846 **Acknowledgements**

847 This work was supported by the Horizon Europe [101079342]; the Slovak  
848 Research and Development Agency [APVV-20-0261]; and the Scientific Grant  
849 Agency of the Slovak Republic [1/0490/23].

850 **References**

- 851 Ahmad, S., Lavin, A., Purdy, S., Agha, Z., 2017. Unsuper-  
852 vised real-time anomaly detection for streaming data. Neuro-  
853 computing 262, 134–147. URL: <https://www.sciencedirect.com/science/article/pii/S0925231217309864>, doi:<https://doi.org/10.1016/j.neucom.2017.04.070>. online Real-Time Learning Strategies for  
855 Data Streams.
- 857 Amarasinghe, K., Kenney, K., Manic, M., 2018. Toward explainable deep  
858 neural network based anomaly detection, in: 2018 11th International Con-  
859 ference on Human System Interaction (HSI), pp. 311–317. doi:[10.1109/HSI.2018.8430788](https://doi.org/10.1109/HSI.2018.8430788).
- 861 Amer, M., Goldstein, M., Abdennadher, S., 2013. Enhancing one-class sup-  
862 port vector machines for unsupervised anomaly detection, in: Proceed-  
863 ings of the ACM SIGKDD Workshop on Outlier Detection and Descrip-  
864 tion, Association for Computing Machinery, New York, NY, USA. pp.  
865 8–15. URL: <https://doi.org/10.1145/2500853.2500857>, doi:[10.1145/2500853.2500857](https://doi.org/10.1145/2500853.2500857).

- 867 Barbosa Roa, N., Travé-Massuyès, L., Grisales-Palacio, V.H., 2019. Dy-  
868 clee: Dynamic clustering for tracking evolving environments. Pat-  
869 tern Recognition 94, 162–186. URL: <https://www.sciencedirect.com/science/article/pii/S0031320319301992>, doi:<https://doi.org/10.1016/j.patcog.2019.05.024>.
- 872 Bosman, H.H., Iacca, G., Tejada, A., Wörtche, H.J., Liotta, A., 2015. En-  
873 sembles of incremental learners to detect anomalies in ad hoc sensor net-  
874 works. Ad Hoc Networks 35, 14–36. URL: <https://www.sciencedirect.com/science/article/pii/S1570870515001481>, doi:<https://doi.org/10.1016/j.adhoc.2015.07.013>. special Issue on Big Data Inspired Data  
876 Sensing, Processing and Networking Technologies.
- 878 Brito, L.C., Susto, G.A., Brito, J.N., Duarte, M.A.V., 2023. Fault diag-  
879 nosis using explainable ai: A transfer learning-based approach for ro-  
880 tating machinery exploiting augmented synthetic data. Expert Systems  
881 with Applications 232, 120860. URL: <https://www.sciencedirect.com/science/article/pii/S0957417423013623>, doi:<https://doi.org/10.1016/j.eswa.2023.120860>.
- 884 Carletti, M., Masiero, C., Beghi, A., Susto, G.A., 2019. Explainable machine  
885 learning in industry 4.0: Evaluating feature importance in anomaly detec-  
886 tion to enable root cause analysis, in: 2019 IEEE International Conference  
887 on Systems, Man and Cybernetics (SMC), pp. 21–26. doi:[10.1109/SMC.2019.8913901](https://doi.org/10.1109/SMC.2019.8913901).
- 889 Chandola, V., Banerjee, A., Kumar, V., 2009. Anomaly detection: A sur-  
890vey. ACM Comput. Surv. 41. URL: <https://doi.org/10.1145/1541880.1541882>, doi:[10.1145/1541880.1541882](https://doi.org/10.1145/1541880.1541882).
- 892 Cook, A.A., Misirlı, G., Fan, Z., 2020. Anomaly detection for iot time-  
893 series data: A survey. IEEE Internet of Things Journal 7, 6481–6494.  
894 doi:[10.1109/JIOT.2019.2958185](https://doi.org/10.1109/JIOT.2019.2958185).
- 895 Du, X., Chen, J., Yu, J., Li, S., Tan, Q., 2024. Generative adversarial nets  
896 for unsupervised outlier detection. Expert Systems with Applications 236,  
897 121161. URL: <https://www.sciencedirect.com/science/article/pii/S0957417423016639>, doi:<https://doi.org/10.1016/j.eswa.2023.121161>.

- 900 Fan, C., Sun, Y., Zhao, Y., Song, M., Wang, J., 2019. Deep learning-  
901 based feature engineering methods for improved building energy predic-  
902 tion. Applied Energy 240, 35–45. URL: <https://www.sciencedirect.com/science/article/pii/S0306261919303496>, doi:<https://doi.org/10.1016/j.apenergy.2019.02.052>.
- 905 Genz, A., 2000. Numerical computation of multivariate normal probabili-  
906 ties. Journal of Computational and Graphical Statistics 1. doi:[10.1080/10618600.1992.10477010](https://doi.org/10.1080/10618600.1992.10477010).
- 908 Gözüaçık, Ö., Can, F., 2021. Concept learning using one-class classi-  
909 fiers for implicit drift detection in evolving data streams. Artificial  
910 Intelligence Review 54, 3725–3747. URL: <https://doi.org/10.1007/s10462-020-09939-x>, doi:[10.1007/s10462-020-09939-x](https://doi.org/10.1007/s10462-020-09939-x).
- 912 Huang, J., Cheng, D., Zhang, S., 2023. A novel outlier detecting algorithm  
913 based on the outlier turning points. Expert Systems with Applications 231,  
914 120799. URL: <https://www.sciencedirect.com/science/article/pii/S0957417423013015>, doi:<https://doi.org/10.1016/j.eswa.2023.120799>.
- 917 Iglesias Vázquez, F., Hartl, A., Zseby, T., Zimek, A., 2023. Anomaly detec-  
918 tion in streaming data: A comparison and evaluation study. Expert Sys-  
919 tems with Applications 233, 120994. URL: <https://www.sciencedirect.com/science/article/pii/S0957417423014963>, doi:<https://doi.org/10.1016/j.eswa.2023.120994>.
- 922 Katser, I.D., Kozitsin, V.O., 2020. Skoltech anomaly benchmark  
923 (skab). <https://www.kaggle.com/dsv/1693952>. doi:[10.34740/KAGGLE/DSV/1693952](https://doi.org/10.34740/KAGGLE/DSV/1693952).
- 925 Kejariwal, A., 2015. Introducing practical and ro-  
926 bust anomaly detection in a time series. URL:  
927 [https://blog.twitter.com/engineering/en\\_us/a/2015/introducing-practical-and-robust-anomaly-detection-in-a-time-series](https://blog.twitter.com/engineering/en_us/a/2015/introducing-practical-and-robust-anomaly-detection-in-a-time-series).
- 929 Krawczyk, B., Woźniak, M., 2015. One-class classifiers with incre-  
930 mental learning and forgetting for data streams with concept drift.  
931 Soft Computing 19, 3387–3400. URL: <https://doi.org/10.1007/s00500-014-1492-5>.

- 933 Laptev, N., Amizadeh, S., Flint, I., 2015. Generic and scalable frame-  
934 work for automated time-series anomaly detection, in: Proceedings of  
935 the 21th ACM SIGKDD International Conference on Knowledge Discov-  
936 ery and Data Mining, Association for Computing Machinery, New York,  
937 NY, USA. pp. 1939–1947. URL: <https://doi.org/10.1145/2783258.2788611>, doi:10.1145/2783258.2788611.
- 938
- 939 Li, J., Liu, Z., 2024. Attribute-weighted outlier detection for mixed  
940 data based on parallel mutual information. Expert Systems with  
941 Applications 236, 121304. URL: <https://www.sciencedirect.com/science/article/pii/S0957417423018067>, doi:<https://doi.org/10.1016/j.eswa.2023.121304>.
- 942
- 943
- 944 Liu, B., Xiao, Y., Yu, P.S., Cao, L., Zhang, Y., Hao, Z., 2014. Uncertain  
945 one-class learning and concept summarization learning on uncertain data  
946 streams. IEEE Transactions on Knowledge and Data Engineering 26, 468–  
947 484. doi:10.1109/TKDE.2012.235.
- 948
- 949 Lyu, Y., Li, W., Wang, Y., Sun, S., Wang, C., 2020. Rmhsforest: Relative  
950 mass and half-space tree based forest for anomaly detection. Chinese Jour-  
951 nal of Electronics 29, 1093–1101. doi:<https://doi.org/10.1049/cje.2020.09.010>.
- 952
- 953 Miao, X., Liu, Y., Zhao, H., Li, C., 2019. Distributed online one-class support  
954 vector machine for anomaly detection over networks. IEEE Transactions  
955 on Cybernetics 49, 1475–1488. doi:10.1109/TCYB.2018.2804940.
- 956
- 957 Mishra, S., Datta-Gupta, A., 2018. Chapter 3 - distributions and models  
958 thereof, in: Mishra, S., Datta-Gupta, A. (Eds.), Applied Statistical  
959 Modeling and Data Analytics. Elsevier, pp. 31–67. URL: <https://www.sciencedirect.com/science/article/pii/B9780128032794000031>,  
doi:<https://doi.org/10.1016/B978-0-12-803279-4.00003-1>.
- 960
- 961 Montiel, J., Halford, M., Mastelini, S.M., Bolmier, G., Sourty, R., Vaysse,  
962 R., Zouitine, A., Gomes, H.M., Read, J., Abdessalem, T., Bifet, A., 2021.  
963 River: machine learning for streaming data in python. Journal of Ma-  
964 chine Learning Research 22, 1–8. URL: <http://jmlr.org/papers/v22/20-1380.html>.

- 965 Nguyen, Q.P., Lim, K.W., Divakaran, D.M., Low, K.H., Chan, M.C., 2019.  
966 Gee: A gradient-based explainable variational autoencoder for network  
967 anomaly detection, in: 2019 IEEE Conference on Communications and  
968 Network Security (CNS), pp. 91–99. doi:10.1109/CNS.2019.8802833.
- 969 Nogueira, F., 2014. Bayesian Optimization: Open source constrained  
970 global optimization tool for Python. URL: <https://github.com/fmfn/BayesianOptimization>.
- 972 Pannu, H.S., Liu, J., Fu, S., 2012. Aad: Adaptive anomaly detection system  
973 for cloud computing infrastructures, in: 2012 IEEE 31st Symposium on  
974 Reliable Distributed Systems, pp. 396–397. doi:10.1109/SRDS.2012.3.
- 975 Ruff, L., Kauffmann, J.R., Vandermeulen, R.A., Montavon, G., Samek, W.,  
976 Kloft, M., Dietterich, T.G., Müller, K.R., 2021. A unifying review of deep  
977 and shallow anomaly detection. Proceedings of the IEEE 109, 756–795.  
978 doi:10.1109/JPROC.2021.3052449.
- 979 Salehi, M., Rashidi, L., 2018. A survey on anomaly detection in evolving  
980 data: [with application to forest fire risk prediction]. SIGKDD Explor.  
981 Newsl. 20, 13–23. URL: <https://doi.org/10.1145/3229329.3229332>,  
982 doi:10.1145/3229329.3229332.
- 983 Stauffer, T., Chastain-Knight, D., 2021. Do not let your safe oper-  
984 ating limits leave you s-o-l (out of luck). Process Safety Progress  
985 40, e12163. URL: <https://aiche.onlinelibrary.wiley.com/doi/abs/10.1002/prs.12163>,  
986 doi:<https://doi.org/10.1002/prs.12163>, arXiv:<https://aiche.onlinelibrary.wiley.com/doi/pdf/10.1002/prs.12163>.
- 988 Steenwinckel, B., 2018. Adaptive anomaly detection and root cause analy-  
989 sis by fusing semantics and machine learning, in: Gangemi, A., Gentile,  
990 A.L., Nuzzolese, A.G., Rudolph, S., Maleshkova, M., Paulheim, H., Pan,  
991 J.Z., Alam, M. (Eds.), The Semantic Web: ESWC 2018 Satellite Events,  
992 Springer International Publishing, Cham. pp. 272–282.
- 993 Steenwinckel, B., De Paepe, D., Vanden Hautte, S., Heyvaert, P., Bente-  
994 frit, M., Moens, P., Dimou, A., Van Den Bossche, B., De Turck, F.,  
995 Van Hoecke, S., Ongena, F., 2021. Flags: A methodology for adap-  
996 tive anomaly detection and root cause analysis on sensor data streams  
997 by fusing expert knowledge with machine learning. Future Generation

- 998 Computer Systems 116, 30–48. URL: <https://www.sciencedirect.com/science/article/pii/S0167739X20329927>, doi:<https://doi.org/10.1016/j.future.2020.10.015>.
- 1001 Talagala, P.D., Hyndman, R.J., Smith-Miles, K., 2021. Anomaly  
1002 detection in high-dimensional data. Journal of Computational  
1003 and Graphical Statistics 30, 360–374. URL: <https://doi.org/10.1080/10618600.2020.1807997>,  
1004 doi:[10.1080/10618600.2020.1807997](https://doi.org/10.1080/10618600.2020.1807997),  
1005 arXiv:<https://doi.org/10.1080/10618600.2020.1807997>.
- 1006 Tartakovsky, A.G., Polunchenko, A.S., Sokolov, G., 2013. Efficient computer  
1007 network anomaly detection by changepoint detection methods. IEEE Journal  
1008 of Selected Topics in Signal Processing 7, 4–11. doi:[10.1109/JSTSP.2012.2233713](https://doi.org/10.1109/JSTSP.2012.2233713).
- 1009
- 1010 Wadinger, M., Kvasnica, M., 2023. Real-time outlier detection with dynamic  
1011 process limits, in: 2023 24th International Conference on Process Control  
1012 (PC), pp. 138–143. doi:[10.1109/PC58330.2023.10217717](https://doi.org/10.1109/PC58330.2023.10217717).
- 1013 Welford, B.P., 1962. Note on a method for calculating corrected sums of  
1014 squares and products. Technometrics 4, 419–420. doi:[10.1080/00401706.1962.10490022](https://doi.org/10.1080/00401706.1962.10490022).
- 1015
- 1016 Wetzig, R., Gulenko, A., Schmidt, F., 2019. Unsupervised anomaly alerting  
1017 for iot-gateway monitoring using adaptive thresholds and half-space  
1018 trees, in: 2019 Sixth International Conference on Internet of Things: Sys-  
1019 tems, Management and Security (IOTSMS), pp. 161–168. doi:[10.1109/IOTSMS48152.2019.8939201](https://doi.org/10.1109/IOTSMS48152.2019.8939201).
- 1020
- 1021 Wu, H., He, J., Tömösközi, M., Xiang, Z., Fitzek, F.H., 2021. In-network  
1022 processing for low-latency industrial anomaly detection in softwarized net-  
1023 works, in: 2021 IEEE Global Communications Conference (GLOBECOM),  
1024 pp. 01–07. doi:[10.1109/GLOBECOM46510.2021.9685489](https://doi.org/10.1109/GLOBECOM46510.2021.9685489).
- 1025
- 1026 Wu, Z., Yang, X., Wei, X., Yuan, P., Zhang, Y., Bai, J., 2024. A self-  
1027 supervised anomaly detection algorithm with interpretability. Expert Sys-  
1028 tems with Applications 237, 121539. URL: <https://www.sciencedirect.com/science/article/pii/S0957417423020419>, doi:<https://doi.org/10.1016/j.eswa.2023.121539>.
- 1029

- 1030 Yamanishi, K., Takeuchi, J.i., 2002. A unifying framework for detecting outliers and change points from non-stationary time series data, in: Proceedings of the Eighth ACM SIGKDD International Conference on Knowledge Discovery and Data Mining, Association for Computing Machinery, New York, NY, USA. pp. 676–681. URL: <https://doi.org/10.1145/775047.775148>, doi:10.1145/775047.775148.
- 1031  
1032  
1033  
1034  
1035
- 1036 Yamanishi, K., Takeuchi, J.i., Williams, G., Milne, P., 2004. On-line unsupervised outlier detection using finite mixtures with discounting learning algorithms. *Data Mining and Knowledge Discovery* 8, 275–300. URL: <https://doi.org/10.1023/B:DAMI.0000023676.72185.7c>, doi:10.1023/B:DAMI.0000023676.72185.7c.
- 1037  
1038  
1039  
1040
- 1041 Yang, W.T., Reis, M.S., Borodin, V., Juge, M., Roussy, A., 2022. An interpretable unsupervised bayesian network model for fault detection and diagnosis. *Control Engineering Practice* 127, 105304. URL: <https://www.sciencedirect.com/science/article/pii/S0967066122001502>, doi:<https://doi.org/10.1016/j.conengprac.2022.105304>.
- 1042  
1043  
1044  
1045
- 1046 Zhang, K., Chen, J., Lee, C.G., He, S., 2024. An unsupervised spatiotemporal fusion network augmented with random mask and time-relative information modulation for anomaly detection of machines with multiple measuring points. *Expert Systems with Applications* 237, 121506. URL: <https://www.sciencedirect.com/science/article/pii/S0957417423020080>, doi:<https://doi.org/10.1016/j.eswa.2023.121506>.
- 1047  
1048  
1049  
1050  
1051  
1052
- 1053 Zhang, X., Shi, J., Huang, X., Xiao, F., Yang, M., Huang, J., Yin, X., Sohail Usmani, A., Chen, G., 2023. Towards deep probabilistic graph neural network for natural gas leak detection and localization without labeled anomaly data. *Expert Systems with Applications* 231, 120542. URL: <https://www.sciencedirect.com/science/article/pii/S0957417423010448>, doi:<https://doi.org/10.1016/j.eswa.2023.120542>.
- 1054  
1055  
1056  
1057  
1058  
1059